Redox Biology 52 (2022) 102317

Contents lists available at ScienceDirect

Redox Biology

journal homepage: www.elsevier.com/locate/redox

Inhibition of STAT3-ferroptosis negative regulatory axis suppresses tumor growth and alleviates chemoresistance in gastric cancer

Shumin Ouyang [a,1], Huaxuan Li [a,1], Linlin Lou [a], Qiuyao Huang [a], Zhenhua Zhang [a], Jianshan Mo [a], Min Li [b], Jiaye Lu [a], Kai Zhu [c], Yunjie Chu [c], Wen Ding [a], Jianzheng Zhu [a], Ziyou Lin [a], Lin Zhong [d], Junjian Wang [a], Peibin Yue [e], James Turkson [e], Peiqing Liu [a,***], Yuanxiang Wang [a,**], Xiaolei Zhang [a,*]

[a] National-Local Joint Engineering Laboratory of Druggability and New Drug Evaluation, Guangdong Key Laboratory of Chiral Molecule and Drug Discovery, School of Pharmaceutical Sciences, Sun Yat-Sen University, Guangzhou, 510006, China
[b] SSL Central Hospital of Dongguan City, Dongguan, 523326, China
[c] Innovation Practice Center, Affiliated Hospital, Changchun University of Chinese Medicine, Changchun, 130117, China
[d] Department of Gastrointestinal Surgery, Sun Yat-sen Memorial Hospital, Sun Yat-sen University, Guangzhou, 510120, China
[e] Department of Medicine, Division of Hematology-Oncology, and Samuel Oschin Comprehensive Cancer Institute, Cedars-Sinai Medical Center, Los Angeles, CA, 90048, USA

ARTICLE INFO

Keywords:
Ferroptosis
STAT3 inhibitor
Chemotherapy resistance
Gastric cancer

ABSTRACT

Chemotherapy is still one of the principal treatments for gastric cancer, but the clinical application of 5-FU is limited by drug resistance. Here, we demonstrate that ferroptosis triggered by STAT3 inhibition may provide a novel opportunity to explore a new effective therapeutic strategy for gastric cancer and chemotherapy resistance. We find that ferroptosis negative regulation (FNR) signatures are closely correlated with the progression and chemoresistance of gastric cancer. FNR associated genes (GPX4, SLC7A11, and FTH1) and STAT3 are upregulated in 5-FU resistant cells and xenografts. Further evidence demonstrates that STAT3 binds to consensus DNA response elements in the promoters of the FNR associated genes (GPX4, SLC7A11, and FTH1) and regulates their expression, thereby establishing a negative STAT3-ferroptosis regulatory axis in gastric cancer. Genetic inhibition of STAT3 activity triggers ferroptosis through lipid peroxidation and Fe^{2+} accumulation in gastric cancer cells. We further develop a potent and selective STAT3 inhibitor, W1131, which demonstrates significant anti-tumor effects in gastric cancer cell xenograft model, organoids model, and patient-derived xenografts (PDX) model partly by inducing ferroptosis, thus providing a new candidate compound for advanced gastric cancer. Moreover, targeting the STAT3-ferroptosis circuit promotes ferroptosis and restores sensitivity to chemotherapy. Our finding reveals that STAT3 acts as a key negative regulator of ferroptosis in gastric cancer through a multi-pronged mechanism and provides a new therapeutic strategy for advanced gastric cancer and chemotherapy resistance.

1. Introduction

Gastric cancer is the fifth most diagnosed malignancy worldwide [1]. Gastric cancer patients are usually at advanced stages when diagnosed, thus losing the opportunity for surgery and with the poor prognosis. Currently, chemotherapy is still one of the standard therapies for gastric cancer. 5-fluorouracil (5-FU)-based regimens are first-line treatments for gastric cancer chemotherapy [2]. However, many patients still relapse

Abbreviations: 5-FU, 5-fluorouracil; STAT3, Signal transducer and activator of Transcription 3; PDX, patient-derived xenografts; FNR, ferroptosis negative regulation; FPR, ferroptosis positive regulation; 4-HNE, 4-hydroxynonenal; MDA, malondialdehyde.

* Corresponding author.
** Corresponding author.
*** Corresponding author.
E-mail addresses: liupq@mail.sysu.edu.cn (P. Liu), wangyx95@mail.sysu.edu.cn (Y. Wang), zhangxlei5@mail.sysu.edu.cn (X. Zhang).
[1] These authors contributed equally to this work.

https://doi.org/10.1016/j.redox.2022.102317
Received 22 January 2022; Received in revised form 15 April 2022; Accepted 17 April 2022
Available online 21 April 2022
2213-2317/© 2022 The Author(s). Published by Elsevier B.V. This is an open access article under the CC BY-NC-ND license (http://creativecommons.org/licenses/by-nc-nd/4.0/).

after several courses of 5-FU-based chemotherapy due to the rapid emergence of drug resistance, which has become a major clinical problem. Chemoresistance is a hallmark of malignant tumors and a major hurdle for cancer therapy [3]. During the latest decades, targeted therapies and immunotherapy have provided a new approach for the treatment of gastric cancer [1,4]. However, the therapeutic effect of these treatment strategies is indisposed and many obstacles remain, thus having not been thoroughly applied in the treatment of gastric cancer. Therefore, new and effective therapies are urgent for advanced gastric cancer and chemoresistance.

Ferroptosis is a form of cell death that is caused by the iron-dependent accumulation of lipid peroxide and was termed by Dixon et al. for the first time in 2012 [5,6]. There are three hallmarks of ferroptosis: glutathione (GSH) biosynthesis, lipid peroxidation, and iron metabolism. Iron is an essential reactive element for a variety of biological processes, which exists in two oxidation states (ferrous [Fe^{2+}] or ferric [Fe^{3+}]), while Fe^{2+} accumulation is an early signal to initiate ferroptosis [7]. Cancer cells resistant to conventional therapy may be susceptible to ferroptosis, in terms of the current research results [8]. Extensive preclinical evidence suggests that the induction of ferroptosis might be an effective therapeutic strategy to alleviate acquired resistance to chemotherapy and targeted therapy [9–11]. Ferroptosis inducers can also work synergistically with traditional drugs (such as cisplatin) to inhibit tumor growth in mouse models of head and neck cancer [12]. More importantly, the susceptibility of different types of cancer cells to ferroptosis was significantly different [13]. Wang et al. revealed that stearoyl-CoA desaturase 1 (SCD1) inhibits ferroptosis of gastric cancer and promotes tumor growth and migration, potentially by altering cancer stemness and modulating cell cycle-related proteins [14]. A recent study found that cancer-associated fibroblasts (CAFs) secrete exosomal miR-522 to inhibit ferroptosis in cancer cells by targeting arachidonate lipoxygenase 15 (ALOX15) and blocking lipid ROS accumulation in gastric cancer [15]. These studies suggest that gastric cancer may be sensitive to ferroptosis, but the role of ferroptosis in the progression and chemoresistance of gastric cancer has remained largely unexplored.

Signal transducer and activator of Transcription 3 (STAT3) is a key oncogene with dual functions of signal transduction and transcriptional activation [16]. Hyperactivation of STAT3 is a pivotal event in the formation of most human cancers and plays a critical role in cell proliferation, angiogenesis, metastasis, and immunosuppression [17–19]. STAT3 is also aberrantly hyperactivated in gastric cancer and promotes the genesis and development of gastric cancer [20]. Meanwhile, some studies showed that alternatively activated STAT3 plays a prominent role in mediating drug resistance to a broad spectrum of chemotherapies, such as cisplatin [21] and EGFR-TKIs [22,23]. As a transcription factor, STAT3 is also associated with oxidative response [24] and may be a potential regulator of ferroptosis. In a previous study, Gao et al. demonstrated that STAT3 is a positive regulator of ferroptosis in human pancreatic ductal adenocarcinoma (PDAC) cell lines. Furthermore, pharmacological and genetic inhibition of STAT3 blocked erastin-induced ferroptosis in PDAC cells [25]. On the contrary, Liu et al. reported that STAT3 inhibitor BP-1-102 may induce ferroptosis in MG63/DDP cells after being exposed to cisplatin [26]. Acyl-CoA synthetase long-chain family member 4 (ACSL4), a lipid metabolism enzyme required for ferroptosis, resulting in elevated lipid peroxidation and ferroptosis [27]. Brown et al. found that α6β4-mediated Src–STAT3 activation represses expression of ACSL4, rendering the cell unable to undergo to ferroptosis, while inhibition of STAT3 increases the expression of ACSL4 to trigger ferroptosis in breast cancer cells [28]. According to previous studies, it is controversial whether activation or inhibition of STAT3 induce ferroptosis, and the effect may be different in different cancers. Whether and how STAT3 regulates ferroptosis in gastric cancer has been elusive and runs short of systemic study.

Herein, we report that ferroptosis negative regulation (FNR) signatures are associated with the progression and chemoresistance of gastric cancer. STAT3 mediates ferroptosis through binding to consensus response elements in the SLC7A11, GPX4, and FTH1 gene promoters. Inhibition of STAT3 triggers ferroptosis that is accompanied by lipid ROS increase, Fe^{2+} accumulation, GSH/GSSG depletion, and lipid peroxidation in gastric cancer. Given the importance of STAT3 in ferroptosis, we further develop a potent and selective STAT3 inhibitor W1131, which triggers ferroptosis and possesses potent anti-tumor effects in gastric cancer cell subcutaneous xenograft model, organoids model, and PDX model. Moreover, the combination of W1131 and 5-FU re-sensitizes the chemoresistant cancer cells to 5-FU and demonstrates a significantly synergistic tumor growth regression in the organoids model and resistant gastric cancer cell subcutaneous xenograft model.

2. Materials and methods

2.1. Cell lines and patient specimens

Cells were maintained in 37 °C incubators with 5% CO_2. All media used were supplemented with 10% fetal bovine serum (FBS, Gibco, Carlsbad, CA, USA), 50 μg/mL penicillin, and 50 μg/mL streptomycin (Gibco, Carlsbad, CA, USA). HEK-293T cells were maintained in a DMEM medium (Gibco, Carlsbad, CA, USA). MGC803, AGS, HGC27, RWPE-1, and A549 cells were maintained in RPMI-1640 medium (Gibco, Carlsbad, CA, USA). 5-fluorouracil-resistanct MGC803/5-FU cells were obtained by continuous treatment with a low dosage of 5-fluorouracil for 16 weeks. The gastric tumor tissues and the paraffin-embedded specimens were from Sun Yat-sen Memorial Hospital, Sun Yat-sen University.

2.2. Chemicals

Ferrostatin-1(T6500), Liproxstatin-1(T2376), Deferoxamine(DFO, T1637), Z-VAD-FMK(T6013), Necrosulfonamide(T7129) and 5-FU (T0984) were obtained from TargetMol (Shanghai, China). BafilomycinA1(S1413) and Erastin(S7242) were obtained from Selleck (Houston, TX, USA). The Synthetic methods and Routes of W1131 are described in detail in Supplemental Information.

2.3. Immunohistochemistry

For immunohistochemistry (IHC) analysis, gastric cancer specimens tissue slides were deparaffinized, rehydrated through an alcohol series followed by antigen retrieval with sodium citrate buffer. Tumor sections were blocked with 5% normal goat serum with 0.1% Triton X-100 and 3% H_2O_2 in PBS for 60 min at room temperature and then incubated with appropriate primary antibodies at 4 °C overnight. IHC staining was performed with horseradish peroxidase (HRP) conjugates using DAB detection. Nuclei were counterstained with Hoechst. Images were taken with Nikon microscopy.

2.4. Cell viability, colony formation, EDU proliferation, invasion, and apoptosis assays

The cell viability assay was measured using the Cell Counting Kit-8 (CCK-8, B34304, Bimake, USA). AGS, MGC803, HGC27, RWPE-1, and MGC803/5-FU cells were plated into a 96-well plate and cultured overnight. Then, W1131 at different concentration was added to each well, and incubation was continued for another 72 h. Next, 10 μL of CCK-8 solution was added to each well, subsequently, cells were incubated for around 4 h until the color of cells turned orange. The absorbance (OD) was measured by a microplate reader (FLUOstar Omega-ACU, USA) at test and reference wavelengths of 450 nm. The percentage of growth was calculated as Cell viability (%) = [OD (Compound +) – OD (Blank)]/[OD (Compound -) – OD (Blank)] × 100%. Each experiment was repeated in triplicate independently.

The colony formation assay was performed to examine the effect of

Table 1
The sequences of two sense strands of siRNA targeting STAT3.

Name	Sequences
siSTAT3#1	Sense:5′-UCCAGUUUCUUAAUUUGUUGACGGGUC-3′ Antisense: 5′-GACCCGUCAACAAAUUAAGAAACUGGA-3′
siSTAT3#2	Sense: 5′-AUAGUCCUAUCUUCUAUUUGGAUGUCA-3′ Antisense:5′-UGACAUCCAAAUAGAAGAUAGGACUAU-3′

W1131 on cell colony survival. AGS, MGC803 cells were seeded into 6-well plates and cultured overnight. Different concentrations of W1131 were added to each well. After that, the cell culture medium was changed and maintained with the same dose of compounds or DMSO every 3 days until the colonies were visible. The cells were fixed using 4% paraformaldehyde and stained with crystal violet staining solution in around 10–15 days.

The EDU proliferation assay was performed using the BeyoClick™ EdU-488 cell proliferation kit (C0075S, Beyotime, Shanghai, China). Cells were seeded into a 12-well plate with a corresponding concentration of EDU reagent for 3 h. Cells were washed with PBS for 5 min twice, before incubating with 4% paraformaldehyde for 30 min. Then, samples were permeated with 0.3% TritonX-100 in PBS and dyed with the reaction solution. A fluorescence microscope was used to capture the image.

The cell invasion assay was performed in 24-well Transwell® plates (3422-ND, Costar, USA). AGS and MGC803 cells were seeded in the top chamber of the insert with RPIM-1640 culture medium containing 2% FBS and cultured overnight, while the bottom chamber was filled with 500 μL of the same medium. The cells were treated with W1131 or DMSO for 12 h and the medium of the bottom chamber was changed 2% FBS into 20% FBS. Then, the cells in the top chamber were carefully removed by cotton and then washed with PBS twice, and the invaded cells in the bottom chamber were fixed with 4% paraformaldehyde and stained with crystal violet staining solution. Finally, the invaded cells were photographed and calculated. Three representative fields were captured for each condition. All experiments were set in triplicate.

The cell apoptosis assay was detected using an Annexin V-FITC Apoptosis Detection Kit I (BB-4101, BestBio, Shanghai, China) following the manufacturer's protocols. Briefly, the cells were washed twice with cold PBS after trypsinization and washed once with the medium. The precipitation was resuspended by 400 μL of 1 × binding buffer, and then resuspended cells were transferred into 1.5 mL tubes. Then 3 μL of Annexin V-FITC and 5 μL of propidium iodide were added to the resuspended cells with further incubation at room temperature for 15 min in the dark. The analysis was conducted by Guava easyCyte (USA) and FlowJo 7.6 software.

2.5. Plasmid constructions and cell transfection

For overexpression of STAT3, STAT3 cDNA(NM_139276.3) was cloned into vector pLVX-FLAG-puro. For RNA interference, gastric cancer cells with 80% confluence in 6-well plates were transfected with control siRNA or STAT3 siRNA using DharmaFECT (T-2001-03, Dharmacon, USA) according to the manufacturer's protocol. A nonspecific oligonucleotide without complementary to any human gene was used as a negative control. The sequences of two sense strands of siRNA targeting STAT3 are listed in Table 1. All above siRNAs were synthesized by Sangon Biotech (Shanghai, China).

2.6. Western blotting and antibodies

Proteins were lysed from cells or tumor tissues using RIPA buffer (Beyotime, Shanghai, China) containing 50 mM Tris-HCl, pH 7.4, 150 mM NaCl, 1% Triton X-100, 1% Na-deoxycholate, 1 mM EDTA, 0.1% SDS, and supplemented with protease inhibitors (Beyotime, Shanghai, China) and phosphatase inhibitors (Bimake, USA). Protein concentration was determined using Pierce™ BCA Protein Assay Kit (23225, Thermo, USA) before proteins were equally loaded and separated by polyacrylamide gel. Proteins were then transferred to polyvinylidene fluoride membranes (PVDF, IPVH00010, Millipore, USA) and incubated overnight with primary antibodies against β-Actin(sc-47778, Santa Cruz, USA), STAT3 (10253-2-AP, Proteintech, Wuhan, Hubei, China), Bcl-xl(sc-8392, Santa Cruz, USA), Phospho-STAT3(Tyr705) (#9145, Cell Signaling Technology, USA), c-Myc (#5605, Cell Signaling Technology, USA), Mcl-1 (#4572, Cell Signaling Technology, USA), STAT1(10144-2-AP, Proteintech, Wuhan, Hubei, China), Phospho-STAT1(Tyr701)(#9167, Cell Signaling Technology, USA), STAT5(#25656, Cell Signaling Technology, USA), Phospho-STAT5 (Tyr694)(#9351, Cell Signaling Technology, USA), JAK2 (#3230, Cell Signaling Technology, USA), phospho-JAK2(Tyr1007/1008, USA) (#3771, Cell Signaling Technology, USA), AKT (#4685, Cell Signaling Technology, USA), Phospho-AKT(Ser473)(#4060, Cell Signaling Technology,USA), Flag-tag(66008-3-Ig, Proteintech, Wuhan, Hubei, China), HA-tag (#3742, Cell Signaling Technology, USA), GPX4(ab125066, abcam, UK), SLC7A11(A13685, Abclonal, Wuhan, Hubei, China), FTH1 (A1144, Abclonal, Wuhan, Hubei, China), 4-HNE(ab48506, abcam, UK), p53(#2524, Cell Signaling Technology, USA), NRF2(66504-1-Ig, Proteintech, Wuhan, Hubei, China), ACSL4(ab155282, abcam, UK), CathepsinB(12216-1-AP, Proteintech, Wuhan, Hubei, China), MLKL (ab184718, abcam, UK), p358-MLKL(ab187091, abcam, UK), LC-3 (14600-1-AP, Proteintech, Wuhan, Hubei, China), PARP-1(#9532, Cell Signaling Technology, USA), Cleaved Caspase-3(#9664, Cell Signaling Technology, USA). HRP-conjugated secondary antibodies were used and the signal was detected on the Bio-rad chemidoc MP system after incubating with ECL solution.

2.7. RT-PCR

The cDNA was prepared using HifairTM II 1st Strand cDNA Synthesis SuperMix Kit (11123ES60, YEASEN, Shanghai, China) according to the manufacturer's protocol. PCR was performed by a BIO-RAD CFX96™ (Bio-rad, San Diego, USA) in the presence of SYBR Green (11201ES08*, YEASEN, Shanghai, China). A melting-curve analysis was performed after the fluorescence values were collected. The sequences of primers for the qRT-PCR analysis are listed in Table S1. All the above primers were synthesized by Sangon Biotech (Shanghai, China).

2.8. LDH release assay

The LDH release assay was measured using the LDH Release Assay Kit (C0017, Beyotime, Shanghai, China) according to the manufacturer's instructions. The samples were prepared and the OD value was measured at 490 nm.

2.9. Transmission electron microscopy

Cells are collected after centrifuge and the precipitation. Then cells were fixed with 3% glutaraldehyde in 0.1 M phosphate buffer (pH 7.4), followed by the fixation with 1% OsO_4. After dehydration, 60–80 nm thin sections were prepared and stained with uranyl acetate and plumbous nitrate before observation under a JEM-1230 transmission electron microscope (JEOL, Tokyo, Japan). High-resolution digital images were acquired from randomly selected five different fields at each condition.

2.10. MDA assay

MDA assay was conducted using the Lipid Peroxidation MDA Assay Kit (S0131, Beyotime, Shanghai, China) according to the manufacturer's instructions. The samples and standards were prepared and the OD value was measured at 532 nm. MDA concentrations (nmol/ml) were expressed as μmol/mg protein.

2.11. GSH/GSSG assay

The levels of GSH (reduced glutathione)/GSSG (oxidized glutathione disulfide) were measured using a GSH/GSSG ratio detection assay kit (ab205811, abcam, UK) according to the manufacturer's instructions.

2.12. FerroOrange assay

AGS and MGC803 cells were seeded into 15 mm glass-bottom dishes and incubated overnight for detection by confocal microscopy. The cells were plated in a 6-well cell culture plate detection by flow cytometry. Subsequently, cells were pretreated with ferroptosis inhibitors for 1 h and then treated with W1131 or vehicle (DMSO) for 24 h. Plates were washed thrice in HBSS. Next cells were stained in 1 μmol/L Ferroorange (F374, DOJINGO, Japan) in HBSS for 30 min at 37 °C incubator with 5% CO_2 and imaged immediately. Treatments were staggered to ensure precise staining duration. Then, images were captured by Laser Scanning Confocal Microscope FV3000 (Olympus, Japan). Five representative fields were captured for each condition under identical exposure times. And Fluorescence intensity was detected by flow cytometry. Data were collected from at least 10,000 cells per sample.

2.13. Liperfluo assay

AGS and MGC803 cells were seeded into 15 mm glass-bottom cell culture dishes and incubated overnight. Then, cells were treated with W1131 or vehicle (DMSO) for 24 h. Cells were stained in 10 μM Liperfluo (L248, DOJINGO, Japan) in RPMI-1640 medium for 30 min at 37 °C incubator with 5% CO_2 and imaged immediately. Treatments were staggered to ensure precise staining duration. Images were captured by Laser Scanning Confocal Microscope FV3000 (Olympus, Japan). Five representative fields were captured for each condition under identical exposure times.

2.14. BODIPY C11 assay

Cells were pretreated with ferroptosis inhibitors for 1 h and then treated with W1131 or vehicle (DMSO) for 24 h. Then, cells were incubated with 5 μM C11-BODIPY 581/591 (Invitrogen, Carlsbad, CA, USA) in a serum-free medium at 37 °C for 30 min in the dark. Cells then were washed with HBSS. Lipid ROS levels were analyzed on a flow cytometer using a 617 nm filter for C11-BODIPY 581/591 detection. Data were collected from at least 10,000 cells per sample.

2.15. Molecular docking

Briefly, the crystal structure of STAT3 (PDB code: 6NUQ) was downloaded from Protein. Data Bank (http://www.pdb.org). Maestro 11.1 software was employed to dock. Schrödinger's Protein Preparation Wizard was used to prepare the protein structure and Schrödinger's LigPrep was used to prepare molecules for docking. Schrödinger's Receptor Grid Generation was used in the generation of grid files. The grid box was prepared at its SH2 domain, and Schrödinger's Ligand Docking was used for docking of the protein structure and ligand. Protein was considered rigid and small molecules were flexible during the docking process. The XP extra precision was chosen as the vital docking parameter.

2.16. Cellular thermal shift assay

To determine target engagement of STAT3 by W1131 within cells, AGS cells with 70%–80% confluence in 15 cm culture dish were treated with W1131 or vehicle (DMSO) for 1 h. Cells were harvested and washed once with PBS, then suspended in 1 ml of PBS supplemented with proteinase and phosphatase inhibitors (Beyotime, Shanghai, China) and also maintained with the same dose of W1131 or DMSO as initial treatment. The cell suspension was distributed into seven 0.2 mL PCR tubes at different designated temperature. Samples were heated at different designated temperature for 2 min using a 96-well thermal cycler. Tubes were removed and incubated at room temperature for 3 min immediately after heating. Three freeze and thaw cycles in liquid nitrogen were performed to lyse the cells. The tubes were vortexed briefly after each thawing. The cell lysate was collected and cell debris together with precipitated and aggregated proteins was removed by centrifuging samples at 20,000 g for 20 min at 4 °C. Cell lysate samples were boiled for 5 min at 95 °C with loading buffer and subjected to western blotting analysis.

2.17. Surface plasmon resonance analysis

The binding affinity between W1131 and STAT3 protein was analyzed by Biacore 8K and Biacore Insight Evaluation software. Purified STAT3 protein (0.17 mg/mL) was dissolved in PBS and immobilized onto the CM5 chip (GE Healthcare, USA). Several concentrations of compound dissolved in running buffer (1 × PBS with filtration, 2% DMSO) were flown over the chip to produce response signals. The kinetics and affinities were calculated by the Biacore Insight Evolution software, and the results were determined as the binding affinity (K_d).

2.18. Immunoprecipitation

For co-immunoprecipitation experiments, 293T cells were co-transfected with plasmids of HA-STAT3 and Flag-STAT3 using Lipofectamine 2000 (1168019, Invitrogen, Carlsbad, CA, USA). Cells were treated with different concentrations of W1131 for 24 h and stimulated with IL-6 (100 ng/mL) for 1 h. Cells were lysed using RIPA buffer supplemented with protease inhibitors and phosphatase inhibitors. The cell lysates were incubated with Anti-flag Affinity Gel (B23102, Bimake, USA) overnight at 4 °C. The gel was washed by PBST three times and denatured by heating for 5 min at 95 °C with 1 × loading buffer. Then the proteins were resolved on SDS–PAGE, transferred to PVDF membranes, and analyzed with immunoblotting.

2.19. Nuclear translocation

Gastric cancer cells were seeded into 15 mm glass-bottom dishes and cultured overnight. Cells were treated with compounds or vehicle (DMSO) for 12 h. The cells were added 100 ng/mL IL-6 (PeproTech, USA) for 30 min before fixation. Then, cells were fixed with 4% paraformaldehyde for 15 min at room temperature. Plates were washed three times by PBS. Then cells were permeabilized with 0.3% Triton X-100 for 15 min at room temperature, and plates were washed thrice by PBS. The samples were blocked with goat serum (Boster, Wuhan, Hubei, China) for 1 h at room temperature, and then, incubated with Phospho-STAT3 (Tyr705) (#9145, Cell Signaling Technology, USA, 1:100) primary antibody overnight at 4 °C. Plates were washed thrice in PBS. Next, cells were incubated with Alexa Fluor 488 Conjugate (#4412, Cell signaling Technology, USA, 1:5000) for 1 h in the dark. Plates were washed thrice in PBS. Then, the cells were subsequently stained with DAPI (40728ES50, Yeasen) for 10 min. Images were captured by Laser Scanning Confocal Microscope FV3000 (Olympus, Japan). Five representative fields were captured for each condition under the same exposure time.

2.20. Transient transfection and luciferase assays

Transient transfections were performed using Lipofectamine 2000 (1168019, Invitrogen, Carlsbad, CA, USA). The STAT3-dependent luciferase reporter, pGL3-STAT3, contained seven copies of the STAT3-specific binding sequence (AATCCCAGAA) in the C-reactive protein gene promoter. For luciferase reporter gene assays, 293T cells were co-transfected with pGL3-STAT3 (50 ng per well) and STAT3C (50

Table 2
The sequences of GPX4, SLC7A11, and FTH1 genes in reporter-gene assay.

Gene	Primer sequence
GPX4 promoter-WT	F: 5′- CCCTCGAGGGACAACATACAAATCCCAAGCAC -3′ R: 5′- CCAAGCTTCTGAGTTGGGTTTGCTTCTCATC -3′
GPX4 promoter-Mut	F: 5′- GTGGTAGCACATGCCTGTGGTCCCAGCTACTC -3′ R: 5′- CCACAGGCATGTGCTACCACGCCCAGCTAATT -3′
SLC7A11 promoter-WT	F: 5′- CGGCTAGCCCTGCAGGTAACCTCCTTTGG -3′ R: 5′- CCCTCGAG TGTTGAGGAAGGCTTATAGTTGTGTG -3′
SLC7A11 promoter-Mut	F: 5′- GCTTTAAATCTCTGGGGGGGTCTGTTCCG -3′ R: 5′- CCCCCAGAGATTTAAAGCAACTCGTAGTGAGC -3′
FTH1 promoter-WT	F: 5′- CGGCTAGCTGGGAAAACTGATTCCACTGATC -3′ R: 5′- CCAAGCTT AGATCAACCTGGAGCTCTACGC -3′
FTH1 promoter-Mut	F: 5′-TCTCAGGGTACAGCCGAGGGGAACCAGCTG -3′ F: 5′- CCCTCGGCTGTACCCTGAGAATGCTCCCTC -3′

Table 3
The sequences of GPX4, SLC7A11, and FTH1 genes in ChIP-qPCR analysis.

Gene	Primer sequence
GPX4 promoter	F: 5′-AATCCAAACCCCTGCCTGTA-3′ R: 5′-CGCGGTATGTGCTCAGAAAA-3′
SLC7A11 promoter	F: 5′-CAAACCAGCTCAGCTTCCTC-3′ R: 5′-TTGAGCAACAAGCTCCTCCT-3′
FTH1 promoter	F: 5′-TTGCCCAGTAACTGTCGG-3′ R: 5′-GGGAGGTGGCTTATCTTGT-3′

ng per well) plasmids. TKRL plasmid (40 ng per well) was used as an internal control. The transfected cells were treated with W1131 for 24 h before being harvested for luciferase assays. Luciferase activity was performed following the Dual-Luciferase Reporter Assay System introduction (Promega Corp, USA).

2.21. RNA-seq data analysis

Total RNA was extracted by TRizol (ThermoFisher, USA) from AGS cells treated with W1131 or vehicle (DMSO) for 48 h and RNase-free DNase I to remove genomic DNA contamination. RNA integrity was evaluated with a 1.0% agarose gel. Thereafter, the quality and quantity of RNA were assessed using a NanoPhotometer® spectrophotometer (IMPLEN, CA, USA). The high-quality RNA samples were subsequently submitted to the Sangon Biotech (Shanghai, China) for library preparation and sequencing. Sequencing libraries were generated using VAHTSTM mRNA-seq V2 Library Prep Kit for Illumina® following the manufacturer's recommendations and index codes were added to attribute sequences to each sample. The libraries were then quantified and pooled. Paired-end sequencing of the library was performed on the HiSeq XTen sequencers (Illumina, San Diego, CA). FastQC (version 0.11.2) was used for evaluating the quality of sequenced data. Clean reads were mapped to the reference genome by HISAT2 (version 2.0) with default parameters. RSeQC (version 2.6.1) was used to analyze the alignment results. Gene expression values of the transcripts were computed by StringTie (version 1.3.3b). Library preparation and high-throughput sequencing were performed by Sangon Biotech (Shanghai, China).

2.22. Reporter constructs and reporter-gene assays

GPX4 reporter-gene assays were performed by transfecting 293T cells with pGL3-GPX4, STAT3C, and pCMV-β-gal for normalization. The GPX4 mutant form (GPX4 Mut) contains sequences mutated from ATGCCTGTAAT to ATGCCTGTGGT. SLC7A11 reporter-gene assays were performed by transfecting 293T cells with pGL3-SLC7A11, STAT3C, and pCMV-β-gal for normalization. The SLC7A11 mutant form (SLC7A11 Mut) contains sequences mutated from TCTCTGGGAAG to ATGCCTGTGGT. FTH1 reporter-gene assays were performed by transfecting 293T cells with pGL3-FTH1, STAT3C, and pCMV-β-gal for normalization. The FTH1 mutant form (FTH1 Mut) contains sequences mutated from CAGCCGAGAAG to CAGCCGAGGGG. Briefly, 293T cells seeded in 96-well plates in phenol red-free DMEM medium were transfected with Lipofectamine 2000 (1168019, Invitrogen, Carlsbad, CA, USA) and the indicated plasmid DNA. 24 h after transfection, transfected cells were treated with W1131 for another 24 h before being harvested for β-galactosidase and luciferase assays. The luciferase and β-galactosidase were then analyzed with a Luciferase Assay Substrate (Promega) and Luminescent β-galactosidase Detection Kit II (Clontech).The primer sequences are listed in Table 2.

2.23. ChIP-qPCR analysis

AGS cells treated with W1131 or vehicle (DMSO) for 48 h, were then fixed with 1% formaldehyde at room temperature for 10 min and washed with ice-cold PBS. Cells were scraped off in buffer I (0.25% Triton X-100/10 mM EDTA/0.5 mM EGTA/10 mM Hepes, pH 6.5). Cell pellets were collected by centrifugation and washed in buffer II (200 mM NaCl/1 mM EDTA/0.5 mM EGTA/10 mM Hepes, pH 6.5). Cell pellets were resuspended in 1 ml of lysis buffer [0.5% SDS/10 mM EDTA/50 mM Tris, pH 8.1/1× protease inhibitor cocktail (Roche Molecular Biochemicals)/1 mg/ml 4-(2-aminoethyl) benzenesulfonyl fluoride] and sonicated four times for a 30-s interval of 0.5-s pulses (Fisher, model 550 Sonic Dismembrator). Cell debris was removed by centrifugation, and the chromatin solutions were diluted 5 × with dilution buffer (1% Triton X-100/2 mM EDTA/150 mM NaCl/20 mM Tris, pH 8.1/1 × protease inhibitor cocktail). Chromatin fragments were immunoprecipitated with specific antibodies overnight at 4 °C. For a 5-ml diluted chromatin solution, the following amounts of antibodies were used: 1 μL of IgG (Millipore, USA) and 2 μg of STAT3 (Proteintech, Wuhan, Hubei, China). Dynabeads TM protein G (1004D, Invitrogen, USA) beads were pre-incubated with Chromatin solution overnight in dilution buffer and washed three times in dilution buffer before using. Immunocomplexes were recovered and eluted. The DNA fragments were purified with a GeneJET Gel Extraction Kit (Thermo, USA) after reverse cross-linking at 65 °C overnight. The immunoprecipitated DNA was analyzed by real-time PCR with SYBR Green on an iCycler instrument. Enrichment of genomic DNA was presented as the percent recovery relative to the input.

The primers are listed in Table 3. All the above primers were synthesized by Sangon Biotech (Shanghai, China).

2.24. Animal experiments

The animal procedures were approved by the Research Ethics Committee of Sun Yat-sen University (SYSU-IACUC-2020-000270; SYSU-IACUC-2021-000139; SYSU-IACUC-2021000149, and SYSU-IACUC-2022-000448) and conducted following the Guide for the Care and Use of Laboratory.

For the MGC803 cell subcutaneous xenograft model, four-week-old BALB/c-nu/nu mice (male, weighing 16–18 g, SPF grade, certification No. SCXK (Nanjing) 2018-0008) were achieved from Nanjing Biomedical Research Institute of Nanjing University (Nanjing, China). Briefly, 2 × 10^6 MGC803 cells were suspended in a total of 100 μL PBS and matrigel (1:1, v/v) and implanted subcutaneously into the dorsal flank of the mice. When the tumor volume was reached about 50 mm^3, the mice were grouped randomly. Then mice were divided into three groups (n = 6) randomly and treated intraperitoneally (i.p.) with 100 μL of either vehicle, W1131 (3 mg/kg), and W1131 (10 mg/kg) for once a day.

For gastric cancer PDX tumor model, four-week-old BALB/c-nu/nu mice (male, weighing 16–18 g, SPF grade, certification No. SCXK (Guang zhou) 2016-0029) were achieved from the Experimental Animal Center of Sun Yat-sen University (Guangdong, China). The characteristics of this patient are as follows: male, 42 years, Asian, primary gastric cancer tumor, AJCC IB/grade 3, surgical sample. The PDX tumors were

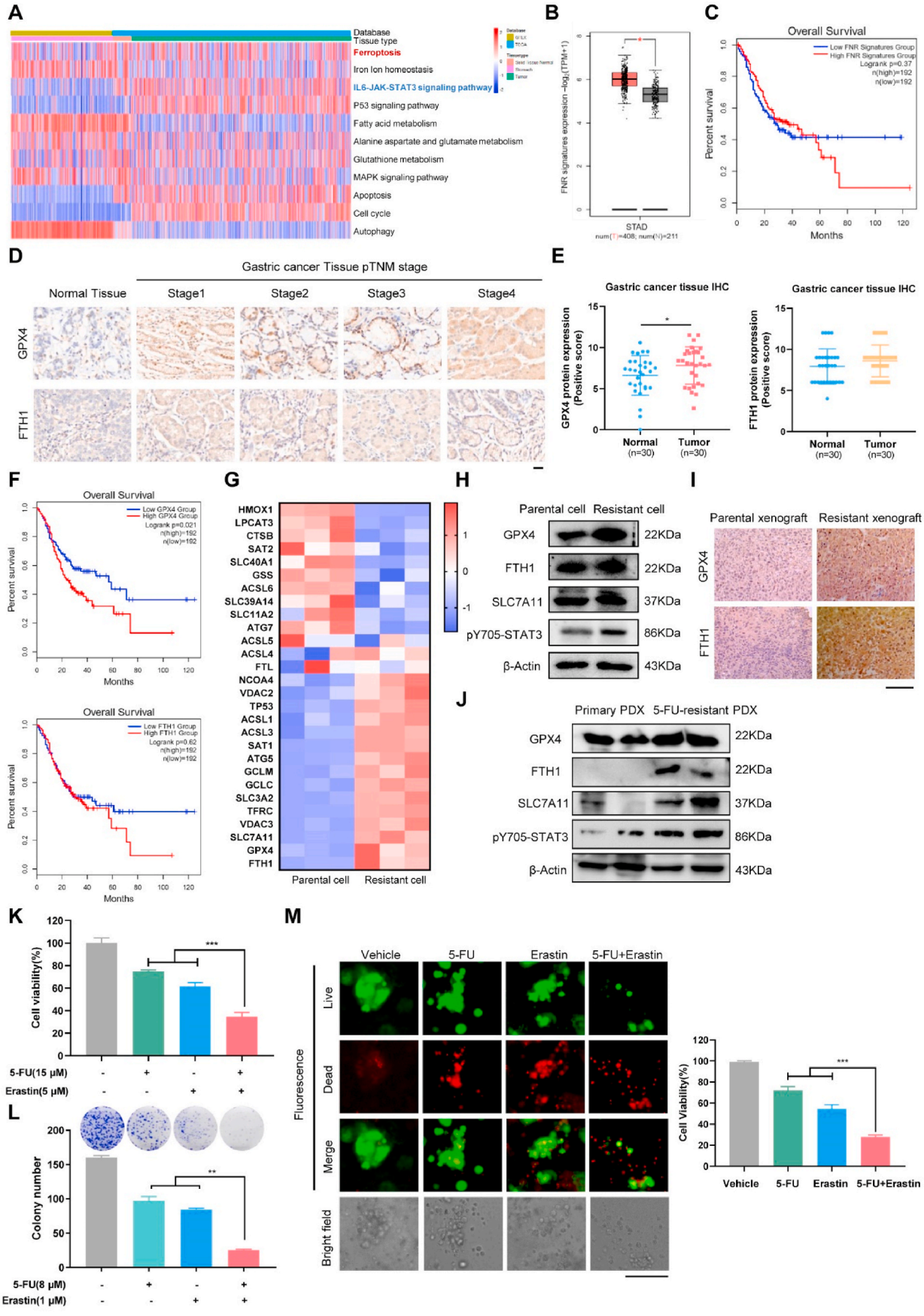

(caption on next page)

Fig. 1. Ferroptosis negative regulation (FNR) signatures is associated with gastric cancer progression and chemoresistance A: Heat map of indicated pathways with data normalized from −2 (blue) to 2 (Red) in 407 gastric cancer tumor tissues and 147 normal gastric tissues or tumor-adjacent tissues. The gene expression datasets were from TCGA and GTEx databases. **B**: Gene expression level of FNR signatures in TCGA gastric cancer tumor and matched TCGA normal stomach tissues along with GTEx data. **C**: Kaplan-Meier survival analysis showed the correlation of FNR signatures expression (Low, n = 192 and High, n = 192) of gastric cancer patients (defined by RNA sequencing with group cutoff in 50%/50% median). **D**: IHC analysis of GPX4 and FTH1 expression in a gastric cancer patient tissue array (n = 30). Representative images are shown. Scale bars = 20 μm. **E**: The IHC signals were scored to evaluate the GPX4 and FTH1 protein expression in gastric cancer tumors compared to the matched normal tissues. **F**: Kaplan-Meier analysis of gastric cancer patients from TCGA project with GPX4 and FTH1 genes high or low expression levels. **G**: RT-PCR analysis of ferroptosis-related genes with cDNA microarrays in MGC803 parental cells and MGC803/5-FU cells. Heatmap indicated the mRNA expression level of ferroptosis-related genes(Z-score). **H**: Immunoblotting analysis of the indicated proteins in MC803 parental cells and MGC803/5-FU cells. **I**: IHC analysis of GPX4 and FTH1 expression in MC803 and MGC803/5-FU xenografts. Scale bars = 100 μm. **J**: Immunoblotting analysis of the indicated proteins in primary gastric cancer PDX and 5-FU-resistant gastric cancer xenografts. **K**: MGC803/5-FU cells were treated with 5-FU (15 μM) and/or erastin (5 μM) as indicated. After 72 h, total viable cells were counted with a Coulter cell counter. **L**: MGC803/5-FU cells were treated with 5-FU (8 μM) and/or Erastian (1 μM) as indicated. 12 days later, colonies were counted. **M**: PDX-derived organoids were treated with DMSO, 5-FU, erastin, and their combination, as indicated. Four days later, representative images were taken under a fluorescence microscope (top three rows) or standard light microscope (bottom row). Scale bars = 100 μm. Cell viability in organoids was measured with CellTiter-Glo. *$P < 0.05$, **$P \leq 0.01$, ***$P < 0.001$, ****$P \leq 0.0001$. n = 3. Student's t-test. All data were shown as means ± s.d. (For interpretation of the references to color in this figure legend, the reader is referred to the Web version of this article.)

propagated in the dorsal flank on both sides of the mice. When the tumor volume was reached about 50 mm^3, the mice were grouped randomly. Then mice were divided into four groups (n = 5) randomly and treated intraperitoneally (i.p.) with either vehicle, W1131 alone, ferrostatin-1 alone, or ferrostatin-1 and W1131 together.

For MGC803/5-FU cell subcutaneous xenograft model, four-week-old BALB/c-nu/nu mice (male, weighing 16–18 g, SPF grade, certification No. SCXK (Nanjing) 2018-0008) were achieved from Nanjing Biomedical Research Institute of Nanjing University (Nanjing, China). Briefly, 2×10^6 MGC803/5-FU cells were suspended in a total of 100 μL PBS and matrigel (1:1, v/v), and implanted subcutaneously into the dorsal flank of the mice. When the tumor volume was reached about 50 mm^3, the mice were grouped randomly. Then mice were divided into three groups (n = 6) randomly and treated intraperitoneally (i.p.) with 100 μL of either vehicle, 5-FU alone, W1131 alone, erastin alone, or 5-FU in combination with erastin or W1131.

For 5-FU-resistant PDX model, four-week-old NCG mice (male, weighing 16–18 g, SPF grade, certification No. SCXK (Nanjing) 2020-0054) were achieved from Nanjing Biomedical Research Institute of Nanjing University (Nanjing, China). Briefly, the PDX tumors were propagated in the dorsal flank on both sides of the mice. When the tumor volume was reached about 50 mm^3, the mice were grouped randomly. Then mice were divided into two groups (n = 5) randomly and treated intraperitoneally (i.p.) with either vehicle or 5-FU.

Tumor volume and body weight were measured two times per week. The volume was calculated with Eq: $V = \pi/6 \times (\text{Length} \times \text{Width}^2)$. The mice were sacrificed at the end of the studies. Tumors were harvested, weighed, and analyzed by immunohistochemistry or immunoblotting assays.

2.25. Organoid culture

Organoids were cultured from PDX xenografts when the tumor size reached ~500 mm^3. Briefly, dissected tumors were finely minced and transferred to a 50 ml centrifuge tube, including a digestion mix consisting of Ad-DMEM/F-12 medium (Gibco, USA) and 1 mg/ml collagenase IV (Sigma, USA), and incubated for 40 min at 37 °C. Isolated organoids were mixed with 5 μL of Matrigel (Costar, USA) and seeded in 96-well plates (Costar, USA). The culture medium contains Ad-DMEM/F-12 with B27 supplement (1 ×), nicotinamide (10 mM), N-acetyl-L-cysteine (1.25 mM), EGF (5 ng/ml), A83- 01 (500 nM), SB202190 (10 μM), Y-27632 (10 μM), Noggin (100 ng/mL), R-Spondin 3 (250 ng/ml), FGF2 (5 ng/ml), FGF 10 (10 ng/ml), penicillin/streptomycin (1 ×) and Glutamine (1 ×). Supplemented culture medium (100 μL) was added per well, and organoids were maintained in a 37 °C humidified atmosphere under 5% CO_2.

2.26. Organoid viability

Organoids were seeded into 96-well plates at 300–500 organoids in 5 μL of Matrigel per well in a total volume of 100 μL of the medium. Serially diluted compounds in 100 μL of medium were added to the cells 24 h later. After 4 days of incubation, Cell-Titer Glo reagents (Promega, USA) were added, and luminescence was measured. After 4 days of incubation, the medium was carefully aspirated and 100 μl of live/dead reagents (US EVERBRIGHT) was added followed by 30 min of incubation at room temperature. A fluorescence microscope was used to capture images of calcein AM (494/517 nm) to represent the live cells, of PI (535/617 nm) to identify the dead cells. The above assays were performed in triplicates.

2.27. Bioinformatics analysis

The gene expression profile datasets GSE13911 and GSE27342 were downloaded from Gene Expression Omnibus (GEO) database. The RNA Seq data of gastric cancer tissue in TCGA database and normal gastric tissue or adjacent gastric tissue in GTEX database were downloaded from the UCSC Xena website (http://xena.ucsc.edu/) and subsequently analyzed by R (Version 3.4, http://www.bioconductor.org) with edgeR package using GSVA method. GSEA analysis was performed using the Java desktop software (http://software.broadinstitute.org/gsea/index.jsp). Genes were ranked according to the shrunken limma $\log_2$ fold changes, and the GSEA tool was used in 'pre-ranked' mode with all default parameters. Bubble chart and volcano plot analysis was performed using the OmicShare tools, an online platform for data analysis (http://www.omicshare.com/tools). A web server for cancer and normal gene expression profiling and interactive analyses, GEPIA (http://gepia.cancer-pku.cn/index.html) and Kaplan-Meier Plotter (https://kmplot.com/analysis/) was recruited to determine the expression of related genes in gastric cancer and the clinical survival of the related genes. The online database of R2: Genomics Analysis and Visualization Platform (https://hgserver1.amc.nl) was applied to determine the correlation between STAT3 and related genes. The open-access database of transcription factor binding profiles-JASPAR 2020 (http://jaspar.genereg.net/) was recruited to predict related motifs.

3. Results

3.1. Ferroptosis negative regulation (FNR) signatures are associated with progression and chemoresistance of gastric cancer

We interrogated the TCGA dataset and GTEx dataset (407 gastric cancer tumor tissues and 147 normal gastric tissues or tumor-adjacent tissues) to explore major cancer pathways that are differentially altered in gastric cancer. The analysis showed that the expression of genes in the IL6-JAK-STAT3 signaling pathway and ferroptosis circuit

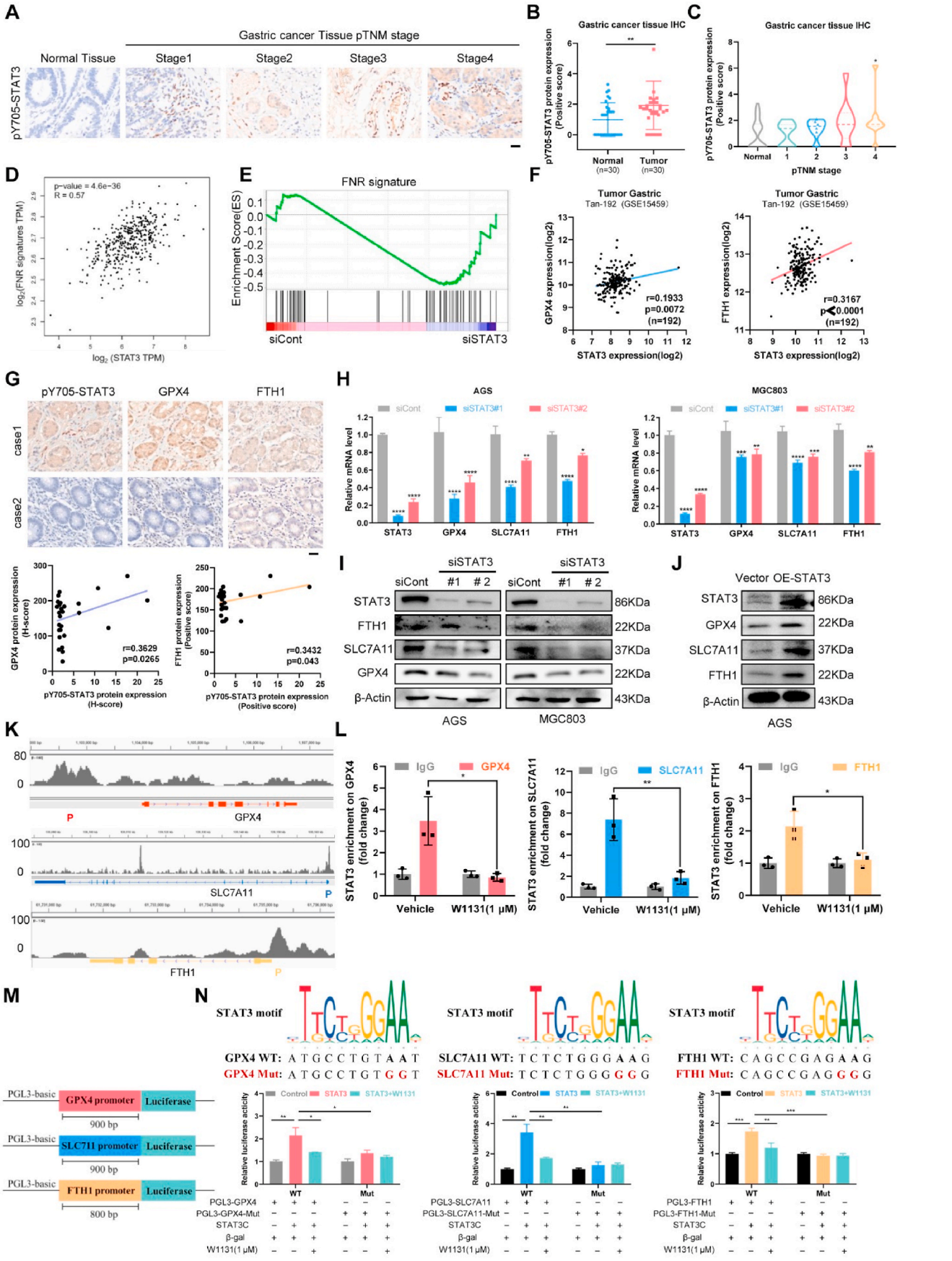

(caption on next page)

Fig. 2. STAT3 mediates ferroptosis through regulation of FNR signatures in gastric cancer A: IHC analysis of pY705-STAT3 expression in a gastric cancer patient tissue array (n = 30). Representative images are shown. Scale bars = 20 μm. **B**: The IHC signals were scored to evaluate the pY705-STAT3 protein expression in gastric cancer tumors compared to the matched normal tissues. **C**: Correlations of pY705-STAT3 expression with pTNM stage of gastric cancer patients according to the IHC signals. **D**: Pearson's correlation analysis of the mRNA levels of STAT3 and FNR signatures in TCGA gastric cancer tumor. **E**: GSEA analysis of RNA seq in AGS cells transfected with siRNAs against STAT3 for 48 h, compared to control siRNA (siCont). **F**: Pearson's correlation analysis of the mRNA levels of STAT3 and the indicated gene in gastric tumor samples from the GEO database. **G**: IHC images of the indicated proteins in human gastric cancer samples. Scale bars = 20 μm. Correlation analysis of the protein levels of pY705-STAT3 and the indicated proteins in patients with gastric cancer by IHC in the bottom. **H**: AGS and MGC803 cells were transfected with control or STAT3 siRNA and cultured for 48 h before being collected for RT-PCR analysis of the indicated genes. **I**: Immunoblotting of the indicated proteins in AGS and MGC803 cells, both treated with control or STAT3 siRNAs for 72 h. **J**: immunoblotting analysis of the indicated proteins in MGC803 cells treated with control or STAT3 overexpression for 72 h. **K**: Genome browser display of STAT3-binding events on promoters of GPX4 gene, SLC7A11 gene and FTH1 gene, data from previous reported ChIP-seq data (GSE117164). **L**: ChIP-qPCR analysis of relative enrichment of STAT3 at the indicated gene promoter in AGS cells treated with vehicle or W1131 for 48 h. Fold change means the indicated enrichment on this gene under influence of W1131 compared to the IgG enrichment in cells treated with vehicle control set as 1. **M**: Promoter of GPX4, SLC7A11, and FTH1 containing human STAT3 motif site was cloned into luciferase reporter vector, respectively. **N**: Sequences of the wild-type and mutant forms of GPX4/SLC7A11/FTH1 linked to reporters (top). GPX4/SLC7A11/FTH1 (wild type or mutated) promoter-luciferase reporter activity changes by STAT3 overexpression or treatment with 1 μM STAT3 inhibitor W1131 in HEK-293T cells for 24 h(bottom). $*P < 0.05$, $**P \leq 0.01$, $***P < 0.001$, $****P \leq 0.0001$. n = 3. Student's t-test. All data were shown as means ± s.d.

displayed a significantly different profile in tumor tissues compared with adjacent normal tissues (Fig. 1A). Ferroptosis-related genes are categorized into ferroptosis positive regulation (FPR) signatures that promote ferroptosis, and ferroptosis negative regulation (FNR) signatures that suppress ferroptosis in the FerrDb database (Fig. S1A). Given the important role of ferroptosis in gastric cancer has remained largely unexplored, we further explored the TCGA and GTEx database and found that the FNR signatures were highly elevated in gastric cancer (Fig. 1B) and significantly associated with low survival rates in gastric cancer patients (Fig. 1C), not FPR or entirety of ferroptosis genes (Figs. S1B and C). Among FNR signatures, GPX4 is a central repressor of ferroptosis in cancer cells, which can directly reduce phospholipid hydroperoxide to hydroxyphospholipid, and protect cells against membrane lipid peroxidation [29,30]. As a member of FNR signatures, FTH1 is an important member of the iron storage protein complex, known as ferritin, which prevents Fe^{2+} from being oxidized by ROS [31]. IHC analysis of 30 clinical human gastric tumors and corresponding adjacent normal gastric tissues confirmed the up-regulation of GPX4 and FTH1 protein in tumor tissues (Fig. 1D and E). Moreover, the level of GPX4 is associated with the stage of cancer progression (Fig. 1D and Fig. S1D), implying that GPX4 is strongly correlated with gastric cancer malignancy. The Kaplan–Meier data indicated that a high level of GPX4 or FTH1 in gastric cancer was markedly associated with poor survival (Fig. 1F), suggesting the important roles of these FNR regulators in gastric cancer.

The chemotherapy based on 5-FU is the standard treatment for patients with gastric cancer. However, many patients still relapse after several courses of 5-FU-based chemotherapy due to the rapid emergence of drug resistance, which has become a major clinical problem [2]. To investigate whether ferroptosis plays a role in 5-FU-resistance, we established a 5-FU resistance cell line using MGC803 cells that were sensitive to 5-FU with an IC_{50} of 5.045 μM MGC803 cells acquired resistance to 5-FU after continuous exposure to 5-FU at low concentration for 16 weeks, and the resistant cells were termed as MGC803/5-FU with an IC_{50} of 55.65 μM (Resistance index = 11.03) (Fig. S1F). Next, we carried out cDNA microarrays analysis, which demonstrated the expression of ferroptosis-related genes in MGC803 and MGC803/5-FU cells. We found that the key genes of FNR signatures including GPX4, FTH1, and SLC7A11 were also markedly upregulated in MGC803/5-FU cells compared with those in the parental MGC803 cells (Fig. 1G). To further confirm the result, we performed Western blot analysis and found that the higher protein levels of GPX4, FTH1, and SLC7A11 were also observed in MGC803/5-FU cells (Fig. 1H). A similar effect was also observed in parental MGC803 xenograft and resistant MGC803/5-FU xenograft (Fig. 1I), suggesting the potential roles of FNR signatures in 5-FU resistance. Moreover, we analyzed these proteins in primary gastric cancer PDX and 5-FU-resistant PDX (Figs. S1G–I and Fig. 1J), and that the protein expression of pY705-STAT3,GPX4, SLC7A11 and FTH1 were increased in 5-FU-resistant PDX (Fig. 1K), which was consistent with the profiles in the cell culture model. It indicates the clinical relevance of the cell culture model for the 5-FU resistance phenotype.

Erastin is used to induce ferroptosis and considered as a 'classical' inducer of this regulated cell death subroutine [32]. Given ferroptosis inducers might work synergistically with chemotherapy drugs and the possible roles of ferroptosis in 5-FU resistance, we next performed experiments to explore whether erastin enhanced the sensitivity of resistant cells to 5-FU. Cell viability assays indicated that combining 5-FU with erastin significantly inhibited the cell proliferation of MGC803/5-FU cells (Fig 1L). Then, colony formation assay also showed that the combination of 5-FU with erastin dramatically inhibited colony survival of MGC803/5-FU cells compared with single treatment (Fig 1M). Given that 3D organoids may closely mimic clinical tumors in response to therapeutics, we treated organoids that were derived from gastric cancer PDX with erastin and 5-FU. Similarly, erastin also enhanced the sensitivity of resistant cells to 5-FU in gastric cancer organoids models (Fig 1N). To evaluate whether long-term administration of 5-FU can directly induce ferroptosis, we performed C11-BODIPY assay and found that 5-FU has no obvious effect on lipid peroxidation in gastric cancer cells (Fig. S1J). We further detected the level of 4-hydroxynonenal (4-HNE) protein to evaluate the effect of long-term treatment of 5-FU on ferroptosis *in vivo*. The results demonstrated that 4-HNE protein adducts did not increase after long-term treatment of 5-FU *in vivo* (Fig. S1K), thus 5-FU may not be a direct ferroptosis inducer even in long-term administration. Together, these results strongly support that the FNR signature is closely related to the development and 5-FU resistance of gastric cancer.

3.2. STAT3 mediates ferroptosis through transcriptional regulation of FNR signatures in gastric cancer

As shown in Fig. 1A, the genes in the IL6-JAK-STAT3 signaling pathway were also highly expressed in tumor tissue of gastric cancer patients. To further explore the potential oncogenic role of STAT3 in gastric cancer, IHC analysis of 30 clinical human gastric tumors and corresponding adjacent normal gastric tissues revealed that pY705-STAT3 is highly expressed in gastric tumor tissue (Fig. 2A and B) and associated with the stage of cancer progression (Fig. 2C). STAT3 mRNA level is also highly expressed in gastric tumor tissue (Fig. S2A) and associated with the stages of gastric cancer (Fig. S2B) by analysis of the GEO database. Additionally, Kaplan–Meier analysis indicated that gastric cancer patients with higher levels of STAT3 presented worse overall survival (Fig. S2C). Moreover, the expression of STAT3 is positively associated with FNR signatures in gastric cancer tumors (Fig. 2D). To explore the role of STAT3 in ferroptosis, we knocked down STAT3 and performed transcriptome analysis. Gene-set enrichment analysis (GSEA) showed that FNR signatures were mediated by STAT3 knockdown (Fig. 2E). Furthermore, IHC analysis of gastric cancer tissues also indicated significant positive correlations between pY705-STAT3 and

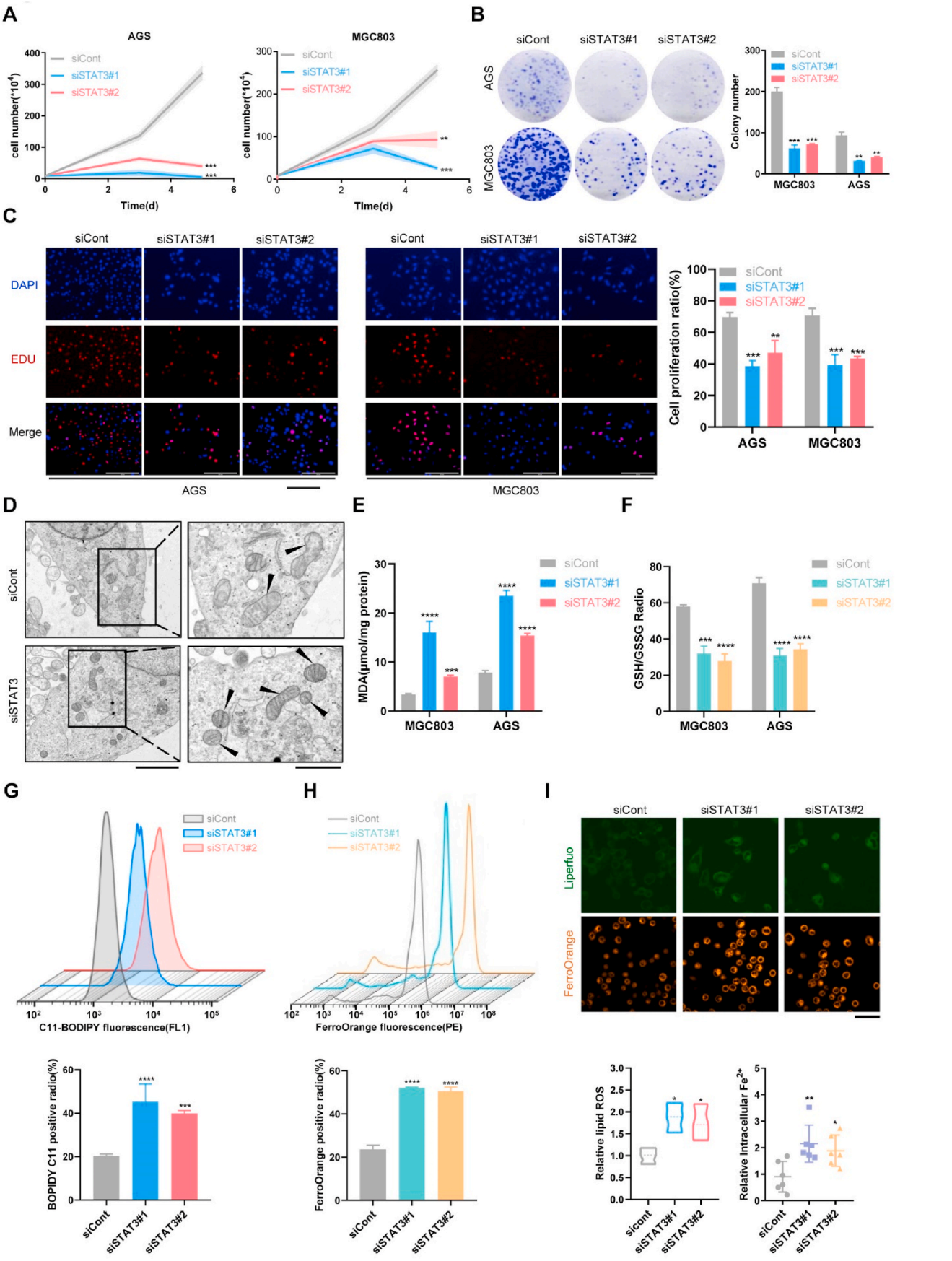

(caption on next page)

Fig. 3. STAT3 inhibition triggers iron-dependent oxidative damage in ferroptosis and suppresses gastric cancer proliferation and survival A: Gastric cancer cells (AGS and MGC803) were transfected with siRNAs against STAT3 (siSTAT3#1 and siSTAT3#2) or control siRNA (siCont). Viable cells were counted at indicated time points. **B**: Gastric cancer cells were infected as in (A). Fourteen days later, colonies were counted. **C**: Gastric cancer cells were infected as in (A). Cell proliferation was determined by Edu cell proliferation assay. Quantification of the signal was shown on the left. Scale bars = 200 μm. **D**: Electron micrographs of STAT3-knockdown in MGC803 cells for 48 h. Scale bars = 2 μm; Scale bars = 1 μm; from left to right, respectively. **E**: AGS and MGC803 cells were transfected with siRNAs against STAT3 (siSTAT3#1 and siSTAT3#2) or control siRNA (siCont) for 48 h, and then intracellular MDA were assayed. **F**: AGS and MGC803 cells were transfected with siRNAs against STAT3 (siSTAT3#1 and siSTAT3#2) or control siRNA (siCont) for 48 h, and then GSH/GSSG ratio were assayed. **G**: C11-BODIPY 581/591 probe was used to detected lipid peroxidation level in AGS cells transfected with siRNAs against STAT3 (siSTAT3#1 and siSTAT3#2) or control siRNA (siCont) for 48 h by flow cytometry. Quantification of C11-BODIPY 581/591(FL1) fluorescence was shown at the bottom. **H**: FerroOrange probe was used to detected intracellular Fe^{2+} level in AGS cells transfected with siRNAs against STAT3 (siSTAT3#1 and siSTAT3#2) or control siRNA (siCont) for 48 h by flow cytometry. Quantification of FerroOrange(PE) fluorescence was shown at the bottom. **I**: Liperfluo and FerroOrange staining for intracellular lipid ROS and Fe^{2+} in MGC803 cells transfected with siRNAs against STAT3 (siSTAT3#1 and siSTAT3#2) or control siRNA (siCont) for 48 h. Shown is one of five representative fields illustrating fluorescence intensity taken at identical exposures for each condition. Scale bars = 50 μm. *$P < 0.05$, **$P \leq 0.01$, ***$P < 0.001$, ****$P \leq 0.0001$. n = 3. Student's t-test. All data were shown as means ± s.d.

GPX4/FTH1, which are key regulators of FNR signature (Fig. 2G). A similar positive correlation between STAT3 and GPX4/FTH1 was also observed through the analysis of the GEO database (Fig. 2F).

Next, we examined whether STAT3 regulates these FNR signatures genes in gastric cancer cells. We performed RT-PCR analysis and found that GPX4, SLC7A11, and FTH1 were significantly down-regulated by STAT3 knockdown in gastric cancer cells (Fig. 2H). Among them, SLC7A11 is a subunit of the cystine/glutamate transporter, which is called system X_c^-. $X_c^{(-)}$ imports cystine into cells and converts it to cysteine, which is used to synthesize GSH [33,34]. Recent studies showed that inhibition of SLC7A11 or GPX4 causes lipid peroxidation and leads to ferroptosis in mammalian cells or tissues [30,35,36]. Moreover, the protein expression of GPX4, SLC7A11, and FTH1 were also inhibited by STAT3 inhibition (Fig. 2I). Therefore, knockdown of STAT3 significantly inhibited GPX4, SLC7A11, and FTH1 at both mRNA and protein levels (Fig. 2H and I). While overexpression of STAT3 promoted the expression of GPX4, SLC7A11, and FTH1 in gastric cancer cells (Fig. 2J). These results imply that the expression of GPX4, SLC7A11, and FTH1 may be regulated by STAT3 in gastric cancer cells.

The previous reported STAT3 ChIP-seq analysis suggested the potential links between STAT3 and GPX4, SLC7A11, and FTH1 genes [37] (Fig. 2K). To assess the regulation of STAT3 on these FNR genes, we performed ChIP-qPCR analysis and found that STAT3 is bound to the promoter of these three genes in gastric cancer cells (Fig 2L). Then, we cloned the promoter of GPX4, SLC7A11, and FTH1 into a dual-luciferase reporter construct, respectively, and performed luciferase reporter-gene assays (Fig 2M). We found that these three genes were highly responsive to STAT3-mediated transactivation (Fig 2N). Finally, we generated the mutant form of GPX4, SLC7A11, and FTH1 promoter by replacing AA with GG in the core motif of human STAT3. Mutations of the putative STAT3 effectively diminished the STAT3-dependent activation (Fig 2N). In addition, it was reported that STAT3 may involve ferroptosis by ACSL4 [28], CathepsinB [25], and STAT3/P53/SLC7A11 pathway [38], we conducted experiments to check these potential mechanisms (Figs. S6A–C). Taken together, these data suggested that STAT3 mediated ferroptosis through transcriptional regulation of FNR signature genes (GPX4, SLC7A11, and FTH1) in gastric cancer.

3.3. STAT3 inhibition triggers iron-dependent oxidative damage in ferroptosis and inhibits gastric cancer cell proliferation and survival

Then, we examined whether STAT3 inhibition contributes to ferroptosis in gastric cancer cells. We knocked down STAT3 in human AGS and MGC803 cells with hyperactivated STAT3 and the knockdown was confirmed by both mRNA and protein levels (Figs. S2D and E). The effects of STAT3 inhibition on cell growth, survival, proliferation, and invasion of gastric cancer cells were also examined (Fig. 3A–C and S2F). Next, we utilized transmission electron microscopy (TEM) to examine the morphological changes in gastric cancer cells transfected with STAT3 siRNAs. The cells which were knocked down of STAT3 exhibited shrunken mitochondria with increased membrane density, which is a characteristic morphologic feature of ferroptosis(Fig. 3D). And knockdown of STAT3 upregulated the level of MDA (malondialdehyde), which is the end product of lipid peroxidation (Fig. 3E). Liperfluo is a lipophilic ROS sensor that provides a rapid, indirect approach to detect lipid ROS [5,6]. The FerroOrange probe is used to detect intracellular Fe^{2+} levels. The results revealed that STAT3 knockdown resulted in increased lipid ROS and enhanced intracellular Fe^{2+} levels in gastric cancer cells by measuring the fluorescence in a confocal microscope (Fig. 3I). To further confirm these effects, we also used flow cytometry to determine the signal of lipid ROS and Fe^{2+}. We found that STAT3 knockdown caused an increase of lipid peroxidation level using the C11-BODIPY probe, which is another probe commonly used to measure lipid ROS (Fig. 3G). Similarly, an increase in Fe^{2+} was also observed in flow cytometry analysis (Fig. 3H). Meanwhile, the knockdown of STAT3 reduced GSH/GSSG ratio in gastric cancer cells, which is considered as a readout for intracellular oxidative damage (Fig. 3F). These results suggested that inhibition of STAT3 could trigger ferroptosis in gastric cancer cells.

3.4. Discovery of a novel and potent STAT3 inhibitor W1131

The above results suggested that STAT3 may serve as a negative regulator of ferroptosis. Therefore, a novel STAT3 inhibitor can act as a ferroptosis-inducing compound for gastric cancer. To this end, we identified a series of compounds based on the privileged structure of 2-phenylimidazo [1,2-a] pyridine for potent and selective STAT3 inhibitors. The detailed structure-activity relationship studies will be reported in a separate publication. W1131 was selected for further study in this article (Fig. 4A and Figs. S3A–B). To determine the potential binding mode of W1131 with STAT3, we performed dock studies using the STAT3 crystal structure (PDB: 6NUQ). The results indicated that the binding model of W1131 with STAT3 (Fig. 4B and Fig. S3C) is similar to that of compound SI-109 [39] (Fig. S3D). The central moiety of W1131 is located at the ligand-binding pocket. The nitrofuran is bound to the pY705 binding site, in which nitro group forms two hydrogen bonds with the Ser611 and Ser613 residue. In addition, the 1,2,3,6-tetrahydropyridine group targets the Leu706 sub pocket and forms a hydrogen bond with Lys658 residue. We then performed surface plasmon resonance (SPR) assays to determine affinity between W1131 and STAT3 protein, with a K_d at 7.55×10^{-6} mol/L (Fig. 4C). To further evaluate W1131 target engagement, we performed the cellular thermal shift assay (CETSA). Drug-protein interaction was examined in the native cellular environment basing on ligand-induced changes in protein thermal stability in CETSA assay [40,41]. W1131 can bind and stabilize STAT3 protein in intact AGS cells (Fig. 4D), suggesting the direct interaction between W1131 and STAT3 protein.

We further demonstrated that W1131 inhibited STAT3 Tyr705 phosphorylation in a time- and dose-dependent manner (Fig. 4E and Fig. S4F) without obvious effect on the activation of STAT1 and STAT5 (Fig. 4F), which confirmed the selectivity of W1131. Similarly, W1131 had no obvious effect on phospho-JAK2 or phospho-AKT levels (Fig. 4G and H). W1131 also suppressed the expression of STAT3 target genes

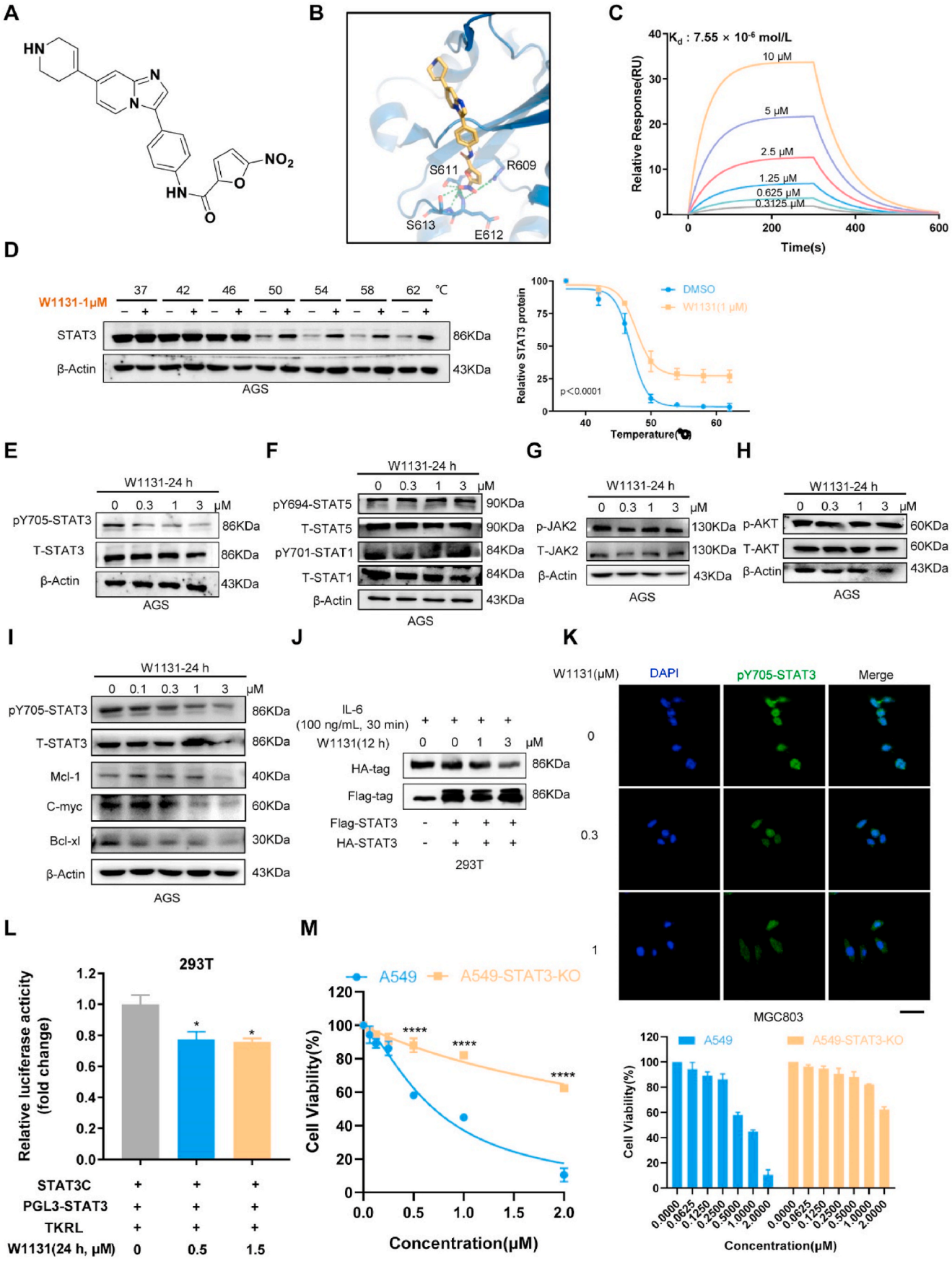

(caption on next page)

Fig. 4. Discovery of a novel and potent STAT3 inhibitor W1131 A: Chemical structures of W1131. **B**: Computational molecular docking analysis to investigate the interaction of W1131 binding to STAT3(PDB:6NUQ). The yellow molecule represents W1131. The docking value of W1131 with STAT3 protein is −5.9166. **C**: SPR analysis of the binding of W1131 to STAT3. **D**: Melt curves of STAT3 protein in CETSA in AGS cells treated with W1131 or vehicle for 1 h. The graph shows the quantification of STAT3 protein versus temperature points based on Western blot analyses. **E**: Western blot was used to detect the expression of STAT3 and pY705-STAT3 in AGS cells treated with vehicle or W1131 for 24 h. **F**: Immunoblotting analysis of the indicated proteins in AGS cells treated with vehicle or W1131 for 24 h. **G**: The expression of JAK2 and pJAK2 in AGS cells treated with vehicle or W1131 for 24 h. **H**: The protein changes of AKT and pAKT in AGS cells treated with vehicle or W1131 for 24 h. **I**: AGS cells treated with vehicle or W1131 for 24 h before being collected for immunoblotting with specific antibodies against indicated proteins. **J**: Immunoprecipitation was used to analyze the dimerization of STAT3 in 293T cells treated with W1131 for 12 h and stimulated with 100 ng/mL IL-6 for 30 min. **K**: Immunofluorescence staining analysis of the translocation of pY705-STAT3(green) in MGC803 cells treated with vehicle or W1131 for 12 h. Scale bars = 50 μm. **L**: Dual-luciferase reporter assay was used to measure the transcriptional activity of 293T cells treated with W1131 for 24 h. Fold change indicates the activities of STAT3 under influence of W1131 compared to the control set as 1. **M**: STAT3-deficient A549 cells constructed by CRISPR-Cas9 treated with vehicle (DMSO) or W1131 for 72 h. Cell viability was measured by CCK8 assay. $^{*}P < 0.05$, $^{**}P \leq 0.01$, $^{***}P < 0.001$, $^{****}P \leq 0.0001$. n = 3. Student's t-test. All data were shown as means ± s.d. (For interpretation of the references to color in this figure legend, the reader is referred to the Web version of this article.)

including c-Myc, Bcl-xl, and Mcl-1, which are associated with cancer cell proliferation and survival (Fig. 4I). To detect the effect of W1131 on the STAT3 dimerization, we co-transfected HA-tagged STAT3 and Flag-tagged STAT3 into HEK-293T cells and performed coimmunoprecipitation assays. We found that W1131 is capable of disrupting STAT3-STAT3 dimerization in intact cells (Fig. 4J). Moreover, W1131 suppressed the nuclear accumulation of pY705-STAT3 in MGC803 cells (Fig. 4K). W1131 inhibited STAT3 transcriptional activity in cell-based luciferase reporter assays (Fig 4L). Furthermore, we generated a STAT3-deficient cell line by CRISPR-Cas9 to further determine the selectivity of W1131 and found that the inhibition of W1131 on cell proliferation was attenuated in STAT3-deficient cells, suggesting the inhibitory effect of W1131 is STAT3 dependent (Fig 4M). Thus, W1131 inhibits STAT3 tyrosine phosphorylation and dimerization, accumulation of nuclear pY705-STAT3, and transcriptional activity. Taken together, these results suggest that W1131 is a novel, selective, and potent STAT3 inhibitor.

3.5. W1131 strongly inhibits cell survival, migration, and invasion in gastric cancer

We next assessed the effects of W1131 on gastric cancer cell growth. W1131 strongly inhibited proliferation of gastric cancer cells with hyperactivated STAT3, whereas it showed weak inhibition on gastric cancer cell HGC27 and human normal cell RWPE-1 without constitutively activated STAT3 (Fig. 5A and Fig. S4B). The basic expression of STAT3 and pY705-STAT3 in these four cells showed in Fig. S4A. Furthermore, W1131 significantly suppressed gastric cancer cell colony formation even at 10 nM (Fig. 5B). The inhibition of cell proliferation by W1131 was demonstrated by the EDU staining assay (Fig. 5C). W1131 manifested stronger and more efficient inhibitory activity of cell viability and survival than a previously reported STAT3 inhibitor SH4-54 [42] (Figs. S4C–D). The effect of W1131 on cancer cell migration and invasion was further investigated. Wound healing assay showed that W1131 significantly reduced cancer cell migration (Figs. 5E and S4E). Transwell assay results demonstrated that W1131 remarkably suppressed the invasion of gastric cancer cells in a dose-dependent manner (Fig. 5D). Next, we performed flow cytometry analysis by Annexin V–FITC staining and found that W1131 indeed induced apoptosis of gastric cancer cells, while the apoptotic percentages were lower than 20% at 3 μM (Fig. S4F), suggesting apoptosis might partly contribute to cancer cell death triggered by W1131. We next carried out LDH release assay with or without inhibitors of apoptosis (Z-VAD-FMK), ferroptosis (ferrostatin-1, liproxstatin-1, and DFO), necrosis(necrosulfonamide), and autophagy(bafilomycinA1) to explore the cell death caused by W1131 treatment. The result demonstrated that the cell death caused by W1131 treatment in gastric cancer cells is varied, and multiple modes of cell death co-exist, which is consistent with the theoretical basis that STAT3 serves as the intersection of multiple signaling pathways and cell functions. Among these cell death caused by W1131, most notably is apoptosis, followed by ferroptosis and necrosis, and autophagy seems to be the least(Fig. 5F). We further found that W1131-caused cell death could be largely reverted by ferroptosis inhibitor ferrostatin-1, liproxstatin-1, and DFO. Similar results were observed in STAT3 knockdown in gastric cancer cells(Fig. 5G). In addition, we also determined important markers of apoptosis, necrosis, and autophagy by western blotting. The expression of apoptosis-related proteins such as cleaved-PARP-1 and cleaved caspase 7 was increased by W1131 (Fig. S4G). Moreover, W1131 increased LC3-II accumulation and pS358-MLKL expression in gastric cancer cells (Fig. S4H, I), which are markers on autophagy and necrosis, respectively. Therefore, the STAT3 inhibitor W1131 shows strong anti-tumor effects through multiple mechanisms *in vitro*.

3.6. W1131 triggers ferroptosis and suppresses GPX4, SLC7A11, and FTH1 expression in gastric cancer

To further investigate whether and how W1131 regulate ferroptosis in gastric cancer cells, we performed RNA-seq transcriptome and gene enrichment analysis. We found that the signaling pathways involved cell cycle, DNA damage response, and oxidative phosphorylation, including IL6-JAK-STAT3 pathway and ferroptosis pathway were regulated by W1131 (Fig. 6A). Further GSEA analysis indicated both the IL6-JAK-STAT3 pathway and FNR signature were inhibited by W1131 (Fig. 6B). 1455 differentially expressed genes (DEGs) between control and W1131 treatment were identified in the volcano plot, of which are 585 up-regulated genes and 870 down-regulated genes, including these FNR signature genes GPX4, SLC7A11, and FTH1 (Fig. 6C). We performed RT-PCR analysis and found that GPX4, SLC7A11 and FTH1 were significantly down-regulated by W1131 (Fig. 6D). The protein expression of GPX4, SLC7A11, and FTH1 was also inhibited by W1131 in a dose-dependent manner (Fig. 6E). Moreover, the ChIP-qPCR analysis indicated that W1131 reduced STAT3 occupancy on the GPX4, SLC7A11, and FTH1 promoter (Fig 2L). Similarly, W1131 effectively diminished the STAT3-dependent activation in a dual-luciferase reporter assay (Fig 2N). These results suggest a new mechanism for STAT3 inhibitors playing function as anti-cancer agents.

Next, we performed experiments to provide further evidence for regulation of W1131 on ferroptosis in gastric cancer cells. Consistent with observations of genetic inhibition of STAT3, W1131 treatment also resulted in smaller mitochondria and higher membrane density, suggesting W1131 induced ferroptosis (Fig. 6F). As expected, we observed that W1131 caused lipid peroxidation by MDA assay, which was reversed by ferroptosis inhibitor ferrostatin-1 and liproxstatin-1 (Fig. 6G). Then, we used Liperfluo, C11-BODIPY, and FerroOrange probe to detect lipid ROS and Fe^{2+} accumulation, and further analyzed by confocal microscopy and flow cytometry. Our results revealed that W1131 significantly promoted lipid ROS formation in gastric cancer cells (Fig. 6I and K), which could be prevented by ferrostatin-1, liproxstatin-1, and DFO (Fig. 6I). And W1131 induced Fe^{2+} accumulation in gastric cancer cells (Fig. 6J and K), which was rescued by the ferroptosis inhibitor ferrostatin-1, liproxstatin-1, and DFO (Fig. 6J). Then, we also evaluated the GSH/GSSG level in gastric cancer cells and found that W1131 treatment result in a decrease in GSH/GSSG ratio (Fig. 6H). To further confirm whether the induction of ferroptosis is common for

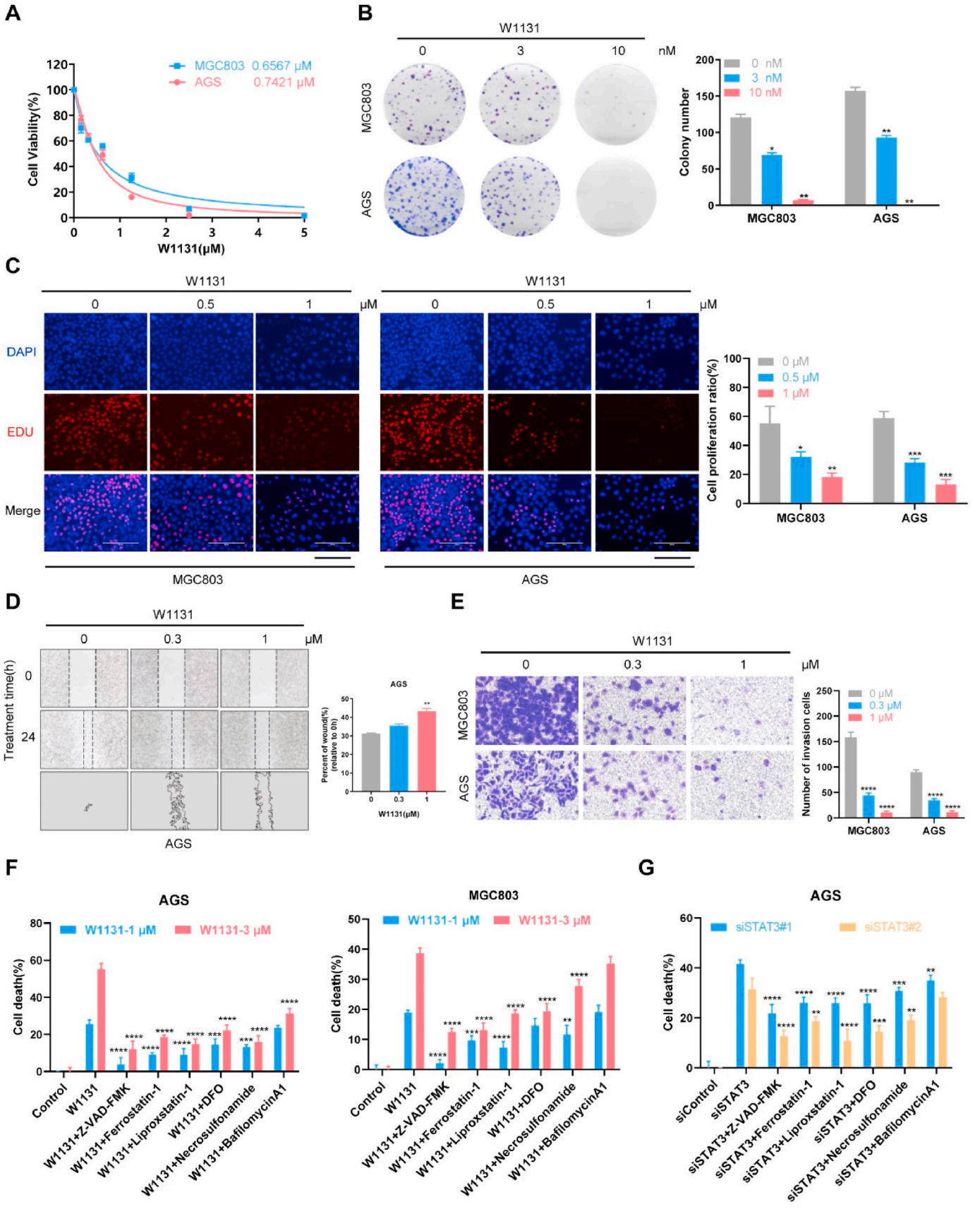

(caption on next page)

Fig. 5. W1131 strongly inhibits cell survival, migration, and invasion in gastric cancer A: Cell viability was measured by CCK8 of AGS and MGC803 cells treated with the indicated concentrations of W1131 for 72 h. **B**: AGS and MGC803 cells were treated with vehicle (DMSO) or the indicated concentrations of W1131. 12 days later, colonies were counted. **C**: Gastric cancer cells were treated with vehicle (DMSO) or the indicated concentrations of W1131 for 48 h. Cell proliferation was determined by EDU cell proliferation assay. Quantification of the signal was shown on the right. **D**: AGS cells were treated with vehicle (DMSO) or the indicated concentrations of W1131. Cell migration was detected by wound healing assay. **E**: AGS and MGC803 cells were treated with vehicle (DMSO) or the indicated concentrations of W1131. Cell invasion was determined by Transwell assay. **F**: AGS and MGC803 cells were treated with vehicle (DMSO) or the indicated concentrations of W1131 in the absence or presence of Z-VAD-FMK(10 μM), Ferrostatin-1(2 μM), Liproxstatin-1(2 μM) and DFO(100 μM), Necrosulfonamide(1 μM) and BafilomycinA1(0.5 μM) for 48 h. Cell death analyses were measured by LDH release assay. **G**: AGS cells were transfected with STAT3 or control siRNA for 48 h and treated with the absence or presence of Z-VAD-FMK(10 μM), Ferrostatin-1(2 μM), Liproxstatin-1(2 μM) and DFO(100 μM), Necrosulfonamide(1 μM) and BafilomycinA1(0.5 μM) for 48 h. Cell death analyses were measured by LDH release assay. $*P < 0.05$, $**P \leq 0.01$, $***P < 0.001$, $****P \leq 0.0001$. n = 3. Student's t-test. All data were shown as means ± s.d.

STAT3 inhibitors, we also use a previously reported STAT3 inhibitor SH4-54 as a positive control to detect lipid peroxidation in gastric cancer cells. As expected, SH4-54 also had a similar effect on an increase of MDA and lipid ROS level as W1131 (Figs. S5A–B). Collectively, these findings demonstrate that ferroptosis triggered by W1131 plays a critical role in the anti-tumor effects of this compound in gastric cancer cells and induction of ferroptosis suggests a new mechanism for STAT3 inhibitors playing function as anti-cancer agents.

3.7. W1131 induces ferroptosis and regresses tumor growth of gastric cancer in vivo

We next evaluated the effects of W1131 on gastric cancer tumor growth. We established the MGC803 subcutaneous xenograft model in BALB/c-nu/nu mice and administrated them with vehicle or W1131 at 3 or 10 mg/kg per day (Fig. 7A). Tumor volume and body weight were monitored every other day. Results showed that W1131 strongly suppressed tumor growth in a dose-dependent manner (Fig. 7B and C), and did not cause significant change of body weight (Fig. S7A) and obvious signs of toxicity, such as loss of appetite, decreased activity, and lethargy during treatment. Histological analysis of the tissues from the lung, heart, liver, kidney, and spleen, further confirmed that there was no obvious toxicity (Figs. S7B–C). Moreover, W1131 significantly decreased STAT3 phosphorylation and its downstream genes including Bcl-xl, Mcl-1, and c-Myc in tumor tissues (Fig. 7F). Immunohistochemical Ki67 staining of the tumor sections suggested that W1131 significantly inhibited cancer cell proliferation (Fig. 7E). W1131 inhibited the expression of GPX4, SLC7A11, and FTH1 in the xenograft tissues, indicating the induction of ferroptosis (Fig. .7E and F). In addition, we performed an iron assay to detect the iron level of tumor tissues and found that W1131 increased iron level *in vivo* (Fig. 7D). Thus, these results suggested that STAT3 inhibition-triggered ferroptosis played an important role in inhibitory effect of W1131in gastric cancer.

Next, we treated organoids derived from gastric cancer PDX with W1131 and ferroptosis inhibitor ferrostatin-1. We found that the organoids were sensitive to W1131 treatment, and the ferroptosis inhibitor ferrostatin-1 could mitigate the anti-tumor effect of W1131(Fig. 7G). Furthermore, we established gastric cancer PDX model in BALB/c-nu/nu mice and administrated it with four regimens (Fig. 7H). Consistent with observations of organoids and *in vitro*, W1131 efficiently reduced gastric cancer tumor growth, and the inhibitory effect was partly attenuated by ferroptosis inhibitor ferrostatin-1 (Fig. .7I and J). Moreover, W1131 inhibited PDX growth, as indicated by Ki67 (Fig. 7K). To provide further evidence, we carried out MDA assay using tumor tissues and found that W1131 upregulated MDA level and the effect was reversed by ferroptosis inhibitor ferrostatin-1 *in vivo* (Fig 7M). Next, we detected the level of 4-HNE, which one of lipid peroxidation products and represents one of the most bioactive and well-studied lipid alkenals [43], which is also a ferroptosis key marker. Our results demonstrated that W1131 significantly increased 4-HNE protein adducts *in vivo*. These results revealed that W1131, as a potent anti-cancer agent, significantly suppressed tumor growth in cancer cell xenograft model, organoids, and PDX model through inhibition of STAT3 signaling pathway and induction of ferroptosis.

3.8. W1131 alleviates chemotherapy resistance of gastric cancer in multiple models

Upregulation of GPX4, SLC7A11, FTH1, and pY705-STAT3 in 5-FU resistant cells (Fig 1H) and 5-FU resistant xenograft (Figs. 1I and 8A) suggests that ferroptosis regulated by STAT3 might contribute to the chemotherapy resistance of gastric cancer. Moreover, knockdown of endogenous STAT3 significantly inhibited cell growth and colony formation in MGC803/5-FU cells (Fig. 8B and C). W1131 also significantly inhibited cell growth of the 5-FU resistant cells (Fig. 8D). Then, we performed cDNA microarrays analysis to assess the expression of ferroptosis-related genes in MGC803/5-FU cells with or without W1131. We found that GPX4, SLC7A11, and FTH1 were upregulated in 5-FU resistant cells(Fig. 1G), and these three genes were down-regulated after treatment with our STAT3 inhibitor W1131 (Fig. 8E). Next, we performed experiments to determine whether W1131 also enhanced 5-FU sensitivity in 5-FU resistant cell lines. The cell viability assays showed that W1131 significantly enhance the sensitivity of MGC803/5-FU cells to 5-FU (Fig. 8F). Colony formation assay also showed that the combination of 5-FU with W1131 significantly inhibited colony survival of MGC803/5-FU cells compared with single treatment (Fig. 8G). A similar synergistic effect was also observed in the gastric cancer organoids models (Fig. 8H). We further evaluated the therapeutic potential for combining ferroptosis inducer erastin or W1131 with 5-FU in MGC803/5-FU cell-derived xenografts. Remarkably, the combinational treatments led to synergistic tumor growth regression in the 5-FU resistant gastric cancer model (Fig. 8I–K), whereas single treatment of STAT3 inhibitor W1131 or ferroptosis inducer erastin only showed moderate and comparable inhibitory effects on the tumor growth compared to that of 5-FU alone. In addition, IHC analysis of xenograft tumors demonstrated that the combined treatment significantly inhibited tumor growth as indicated by Ki67, suppressed STAT3 signaling as indicated by pY705-STAT3, and triggered ferroptosis as indicated by GPX4 (Fig 8L). Together, the results from the cell model, organoids model, and animal model suggest that W1131 significantly alleviated chemotherapy resistance in gastric cancer. The combination of W1131 with chemotherapy drugs can be a new strategy for chemotherapy-resistant gastric cancer.

4. Discussion

Gastric cancer is one of the most common and severe cancer worldwide. The primarily curative approach of nonmetastatic gastric

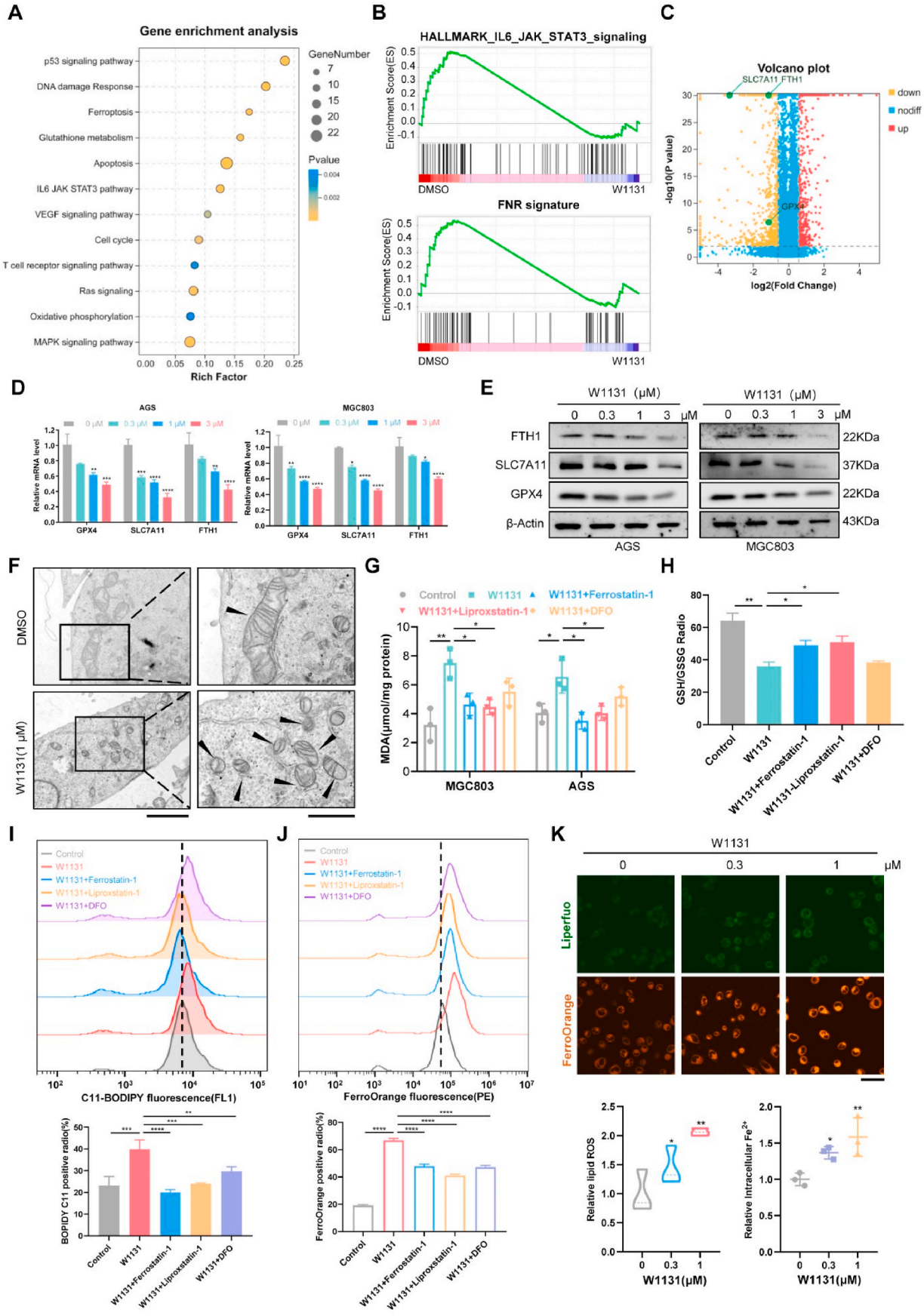

(caption on next page)

Fig. 6. W1131 triggers ferroptosis and inhibited GPX4, SLC7A11, and FTH1 expression in gastric cancer A: Bubble chart displaying the gene enrichment analyses, as detected by RNA-seq in AGS cells treated with W1131(1 μM) for 48 h, as compared to vehicle (DMSO). **B**: GSEA of the FNR signature and IL6 JAK STAT3 pathway in AGS cells treated with W1131(1 μM) for 48 h, as compared to vehicle (DMSO). **C**: Volcano plot showing genome-wide mRNA expression in AGS cells treated with W1131(1 μM) for 48 h, as compared to vehicle (DMSO) ($P < 0.01$; log2 (Fold Change)|>0.585). **D**: RT-PCR analysis of the indicated genes in AGS and MGC803 cells treated with vehicle (DMSO) or W1131 for 48 h. **E**: Immunoblotting analysis of the indicated proteins in AGS cells treated with vehicle (DMSO) or W1131 for 48 h. **F**: Electron micrographs in MGC803 cells treated with vehicle (DMSO) or W1131 for 24 h. **G**: AGS cells were treated with vehicle (DMSO) or W1131 (1 μM) in the absence or presence of Ferrostatin-1(2 μM), Liproxstatin-1(2 μM) and DFO(100 μM) for 24 h, and then intracellular MDA were assayed. **H**: AGS cells were treated with vehicle (DMSO) or W1131 (1 μM) in the absence or presence of Ferrostatin-1(2 μM), Liproxstatin-1(2 μM) and DFO(100 μM) for 24 h, and then GSH/GSSG ratio were assayed. **I**: C11-BODIPY 581/591 probe was used to detected lipid peroxidation level in AGS cells treated with vehicle (DMSO) or W1131 (1 μM) in the absence or presence of Ferrostatin-1(2 μM), Liproxstatin-1(2 μM) and DFO(100 μM) for 24 h by flow cytometry. Quantification of C11-BODIPY 581/591 (FL1) fluorescence was shown. **J**: FerroOrange probe was used to detected intracellular Fe^{2+} level in AGS cells treated with vehicle (DMSO) or W1131 (1 μM) in the absence or presence of Ferrostatin-1(2 μM), Liproxstatin-1(2 μM), and DFO(100 μM) for 24 h by flow cytometry. Quantification of FerroOrange(PE) fluorescence was shown. **K**: Liperfluo and FeroOrange staining for intracellular lipid ROS and Fe^{2+} level in AGS cells treated with vehicle (DMSO) or the indicated concentrations of W1131 for 24 h. Shown is one of five representative fields illustrating fluorescence intensity taken at identical exposures for each condition. Scale bars = 50 μm. *$P < 0.05$, **$P \leq 0.01$, ***$P < 0.001$, ****$P \leq 0.0001$. n = 3. Student's t-test. All data were shown as means ± s.d.

cancer is surgical resection, but the 5-year survival rate diminishes rapidly with increasing stage of disease [44]. Moreover, gastric cancer patients are usually at advanced stages when diagnosed, thus losing the opportunity for surgery and with a poor prognosis, and the interventions such as molecular-targeted therapies and immunotherapy show low clinical response. Although significant progress has been made in the field of neoadjuvant chemotherapies, de novo and acquired resistance to these therapies appear inevitably [45]. 5-FU is the first-line drug for the treatment of gastric cancer but 5-FU resistance occurs in clinical practice frequently. 5-FU resistance may develop due to the various mechanisms and pathways, such as the alterations in drug transport, evasion of apoptosis, regulation of autophagy, cancer stem cell involvement, tumor microenvironment interactions, epigenetic alterations, as well as redox imbalances [46]. In recent years, 5-FU has been used along with other modulators for the treatment of many cancers by targeting apoptosis or other cancer signaling pathway. Apoptosis is also one of the major mechanisms of cell death in response to 5-FU [47]. BAX is an indispensable gateway to mitochondrial dysfunction. The down-regulation of BAX plays an important role acquisition of resistance to 5-FU [48]. Wang et al. found that Andrographolide, a natural diterpenoid from Andrographis paniculate, bound to BAX and triggered mitochondria mediated apoptosis, thus reversing 5-FU resistance [49]. Similarly, apigenin(4′,5,7-trihydroxyflavone), a plant flavone, increased the sensitivity of tumors to 5-FU by activating the mitochondria-mediated apoptosis pathway [50]. Toden et al. reported that curcumin and 5-FU combination synergistically induced apoptosis in 5-FU resistant cells by downregulating the HSP-27 and P-gp expression [51].

In recent years, some publications suggested that ferroptosis might be an effective therapeutic strategy to alleviate chemotherapy resistance [9,10]. Cancer cells which are resistant to conventional treatment might be particularly susceptible to ferroptosis, in terms of the current research results [9], thus the development of novel therapeutic strategies based on ferroptosis may alleviate current gastric cancer resistance. There are ever-growing interests to explore the role of ferroptosis in cancer and exploit ferroptosis to improve cancer prevention, diagnostics, treatment, and prognostics [8,10,52]. In this study, we unravel that the FNR signature is closely related to the development and 5-FU resistance of gastric cancer. We found that the ferroptosis circuit is aberrant expressed in gastric tumors and elevated FNR signature was significantly associated with low survival rates in gastric cancer patients. Furthermore, we found that pY705-STAT3 and GPX4, SLC7A11, and FTH1 were markedly upregulated in 5-FU-resistant gastric cancer cells and xenografts, indicating a potential role of FNR signature in contributing to 5-FU resistance in gastric cancer cells. A combination of 5-FU and ferroptosis inducer erastin demonstrated a significantly synergistic tumor growth regression in the resistant MGC803/5-FU cell and organoids model. It suggests that ferroptosis is closely related to the development and 5-FU resistance of gastric cancer.

We found that there was a positive correlation between STAT3 and FNR signatures GPX4 or FTH1 in human gastric cancer patient samples. Analysis of the GEO database, TCGA database, and gastric cancer patient tissue arrays suggests that STAT3 and FNR signatures are potential drivers for gastric tumorigenesis. The morphological features of ferroptosis are mainly displayed by decreased or vanished mitochondria cristae, a ruptured outer mitochondrial membrane, and a condensed mitochondrial membrane [13,31]. It is reported that GSH depletion, lipid peroxidation, lipid ROS accumulation, and Fe^{2+} accumulation are critical features in ferroptosis [6]. Mitochondria shrinkage, increased mitochondria membrane density, lipid ROS elevation, GSH depletion, lipid peroxidation, and Fe^{2+} accumulations were observed following STAT3 inhibition. We further found that STAT3 may regulate the gene expression of GPX4, FTH1, and SLC7A11 by binding to the promoters. Our data suggested that a high level of GPX4 in gastric cancer was markedly associated with poor survival. Our study also reveals that down-regulation of SLC7A11 and GPX4 by STAT3 inhibition promotes intracellular lipid ROS and MDA level increment and leads to ferroptosis in gastric cancer. Furthermore, we find that STAT3 transcriptionally regulates iron metabolism-related proteins such as FTH1, and mediates intracellular Fe^{2+} levels to induce ferroptosis.

As an oxidative responsive transcriptional factor, STAT3 was reported to be linked to mediation of stress-related ferroptosis [53]. It was reported that activation of Src and STAT3 suppresses the expression of ACSL4 [28]. Another report showed that genetic blockade of STAT3 limited erastin-induced cathepsin B expression [25]. Our results showed that overexpression of STAT3 inhibited the protein expression of ACSL4 in gastric cancer cells but the expression of cathepsin B had no obvious change, whether STAT3 was overexpressed or knocked down. Luo et al. demonstrated that Bavachin (a bioactive compound extracted from the fruit of Psoralea corylifolia) induced ferroptosis by reducing SLC7A11 and GPX4 expression and promoting ROS and MDA accumulation through down regulation of STAT3 and upregulation of P53. Jiang et al. demonstrated that p53 induced ferroptosis by down regulation of SLC7A11 to inhibit cystine transport [54]. Our results suggested that STAT3 inhibitor W1131 can increase p53 expression and inhibit GPX4 and SLC7A11 expression. Further, our results of chip-qPCR and luciferase reporter gene assay indicated STAT3 directly transcriptional regulates GPX4 and SLC7A11 expression in gastric cancer cells. Therefore, knockdown of STAT3 triggered ferroptosis not only by up-regulating p53 to downregulate GPX4 and SLC7A11 expression but also by directly regulating GPX4 and SLC7A11 expression.

Consistently, we found that STAT3 acts as a key negative regulator of ferroptosis in gastric cancer through a multi-pronged mechanism and

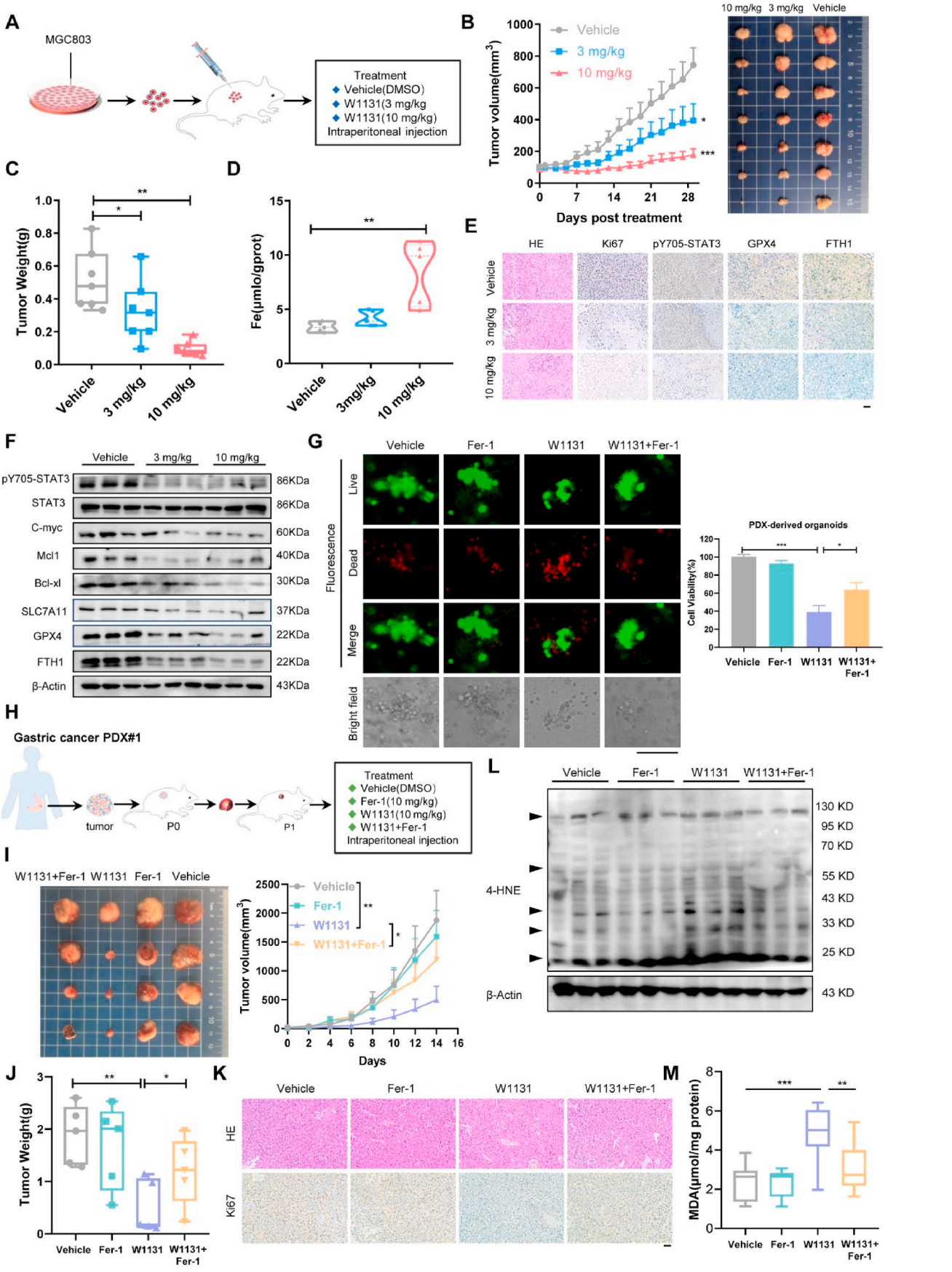

(caption on next page)

Fig. 7. W1131 induces ferroptosis and regresses tumor growth of gastric cancer *in vivo* **A**: Schematics illustrating MGC803 subcutaneous xenograft tumor establishment and treatment. **B–C**: BALB/c-nu/nu mice bearing the MGC803 subcutaneous xenografts (n = 6 mice per group) received vehicle, W1131 (i.p., 3 mg/kg) and W1131 (i.p., 10 mg/kg), as indicated, once daily. Mean tumor volume ± standard error of the mean (SEM) (B), representative tumor images (B), and mean tumor weight ± SEM (C) are shown. **D:** Tissue iron level of the MGC803 xenograft tumors after 28 days of treatment with vehicle or W1131(3 mg/kg and 10 mg/kg). **E**: H&E and IHC images of the indicated proteins in randomly selected MGC803 xenograft tumor section. Scale bars = 100 μm. **F**: Immunoblotting analysis of the indicated proteins in MGC803 xenograft tumors after 28 days of treatment with vehicle or W1131(3 mg/kg and 10 mg/kg) as in (B). **G**: PDX-derived organoids were treated with DMSO, ferrostatin-1, W1131, or a combination of W1131 and ferrostatin-1, as indicated. Four days later, representative images were taken under a fluorescence microscope (top three rows) or standard light microscope (bottom row). Scale bars = 100 μm. Four days later, cell viability in organoids was measured with CellTiter-Glo. **H**: Schematics illustrating gastric cancer PDX mice model establishment and treatment. **I-J**: BALB/c-nu/nu mice bearing the gastric cancer PDX (n = 5 mice per group) received the vehicle, ferrostatin-1 (i.p., 10 mg/kg, once every other day), W1131 (i.p., 10 mg/kg, once daily), or a combination of ferrostatin-1 and W1131, as indicated. Mean tumor volume ± standard error of the mean (SEM) (I), representative tumor images (I), and mean tumor weight ± SEM (J) are shown. **K**: H&E and IHC images of the indicated proteins in the randomly selected PDX tumor section. Scale bars = 100 μm. **L**: Immunoblotting analysis of 4-HNE in gastric cancer PDX tumors. **M**: MAD assay was used to detected lipid peroxidation levels in randomly selected PDX tumor section.*$P < 0.05$, **$P \leq 0.01$, ***$P < 0.001$, ****$P \leq 0.0001$. n = 3. Student's t-test. All data were shown as means ± SEM.

inhibition of STAT3 can trigger ferroptosis through a multi-pronged mechanism associated with lipid peroxidation and iron metabolism. To the best of our knowledge, it is the first to illuminate that STAT3 regulates ferroptosis by directly regulating GPX4, SLC7A11 and FTH1 in gastric cancer. Our work may provide a better understanding for mechanisms of regulation of STAT3 on ferroptosis and a new therapeutic strategy for gastric cancer by targeting the STAT3-ferroptosis circuit.

Given its important role in proliferation, survival, and ferroptosis, STAT3 could serve as an attractive drug target in gastric cancer. Meanwhile, ferroptosis-inducing drugs are attracting more attention for cancer treatment. Several non-peptide SH2 domain inhibitors have been identified and shown to inhibit the growth of cancer cells with hyper-activated STAT3, including BP-1-102, STA-21, STATTIC, S3I-201, STX-0119, and WP1066 [55–61]. OPB-31121 [62,63] and OPB-51602 [64] have all been evaluated in early phase clinical trials. But till now none of the STAT3 inhibitors has been approved for gastric cancer therapy in the clinic. Therefore, it is urgent to develop novel potent and effective STAT3 inhibitors for advanced gastric cancer. To this end, we further developed a novel STAT3 inhibitor W1131 as a gastric cancer therapeutic agent. The target engagement was evaluated by SPR analysis and CETSA assay. We found that W1131 inhibited STAT3 tyrosine phosphorylation, dimerization, accumulation of nuclear pY705-STAT3 and STAT3 transcriptional activity without affecting STAT1 or STAT5. Thus, we identified W1131 as a novel, effective, and selective STAT3 inhibitor. W1131 possessed potent anti-tumor effects and inhibited cell colony survival at the nM level. Moreover, treatment of W1131 showed a pro-ferroptosis phenotype in gastric cancer cells, similar to STAT3 knockdown.

To further investigate the roles of W1131 and the STAT3-ferroptosis axis in the progression and chemoresistance of gastric cancer, we established three different models, including the MGC803 cell xenograft model, gastric cancer organoids model, and PDX model to investigate the anti-tumor effect of W1131 *in vivo* and the role of ferroptosis in W1131-induced-tumor suppression. Our results showed that W1131 triggered ferroptosis and showed significant antitumor effects in gastric cancer. W1131 reduced pY705-STAT3, SLC7A11, GPX4, and FTH1 levels in tumor tissues. Moreover, the combination of 5-FU and W1131 demonstrated a significantly synergistic tumor growth regression in the organoids model and subcutaneous xenograft mouse models to alleviate 5-FU resistance. The results from the cell model, organoids model, and animal model suggest that W1131 alleviates chemotherapy resistance in gastric cancer by induction of ferroptosis. The combination of W1131 with chemotherapy drugs can be a new strategy for chemotherapy-resistant gastric cancer. While it is worthy to note that secondary therapy with other drug such as irinotecan, oxaliplatin and cisplatin should be used as soon as possible, for gastric cancer patients with clinical resistance to 5-FU.

In this study, we systematically demonstrate that the STAT3-ferroptosis circuit plays a critical role in gastric cancer progression and chemoresistance. We discover a novel potent compound W1131, which inhibits STAT3 function, triggers ferroptosis and re-sensitizes the resistant cancer cells to chemotherapy in the organoids model and mouse xenograft model. Our study reveals that STAT3 serves as a key negative regulator of ferroptosis and STAT3 inhibitor can act as a ferroptosis inducer, providing a new therapeutic strategy for advanced gastric cancer and chemotherapy resistance. However, the ferroptosis response is regulated by a complex network of epigenetic transcriptional and post-translational mechanisms [32,65] Therefore, additional important molecular mechanisms by which STAT3 regulates ferroptosis deserve further exploration. A better understanding of the regulatory mechanisms and signaling pathways of ferroptosis, and the searching for biomarkers to facilitate the detection and tracking of ferroptosis will be an active area in the future. This study reveals that targeting ferroptosis through STAT3 inhibition sheds light on new strategies for gastric cancer therapy and chemoresistance.

Study approval

The animal procedures were approved by the Institutional Animal Care and Use Committee of Sun Yat-sen University and followed the Guide for the Care and Use of Laboratory Animals.

Authors' contributions

Conception, design, and supervising of the study: Xiaolei Zhang, Yuanxiang Wang, and Peiqing Liu. Development of methodology and acquisition of data: Shumin Ouyang, Huaxuan Li, Linlin Lou, Qiuyao Huang, Zhenhua Zhang, Jianshan Mo, Jiaye Lu, and Wen Ding. Analysis and interpretation of data: Shumin Ouyang, Qiuyao Huang, Peibin Yue, James Turkson, Linlin Lou, and Zhenhua Zhang. Technical and material support: Min Li, Kai Zhu, Yunjie Chu, Juanjian Wang, Peibin Yue, and James Turkson. Study supervision: Xiaolei Zhang, and Yuanxiang Wang.

Declaration of competing interest

The authors declare that they have no known competing financial interests or personal relationships that could have appeared to influence the work reported in this paper.

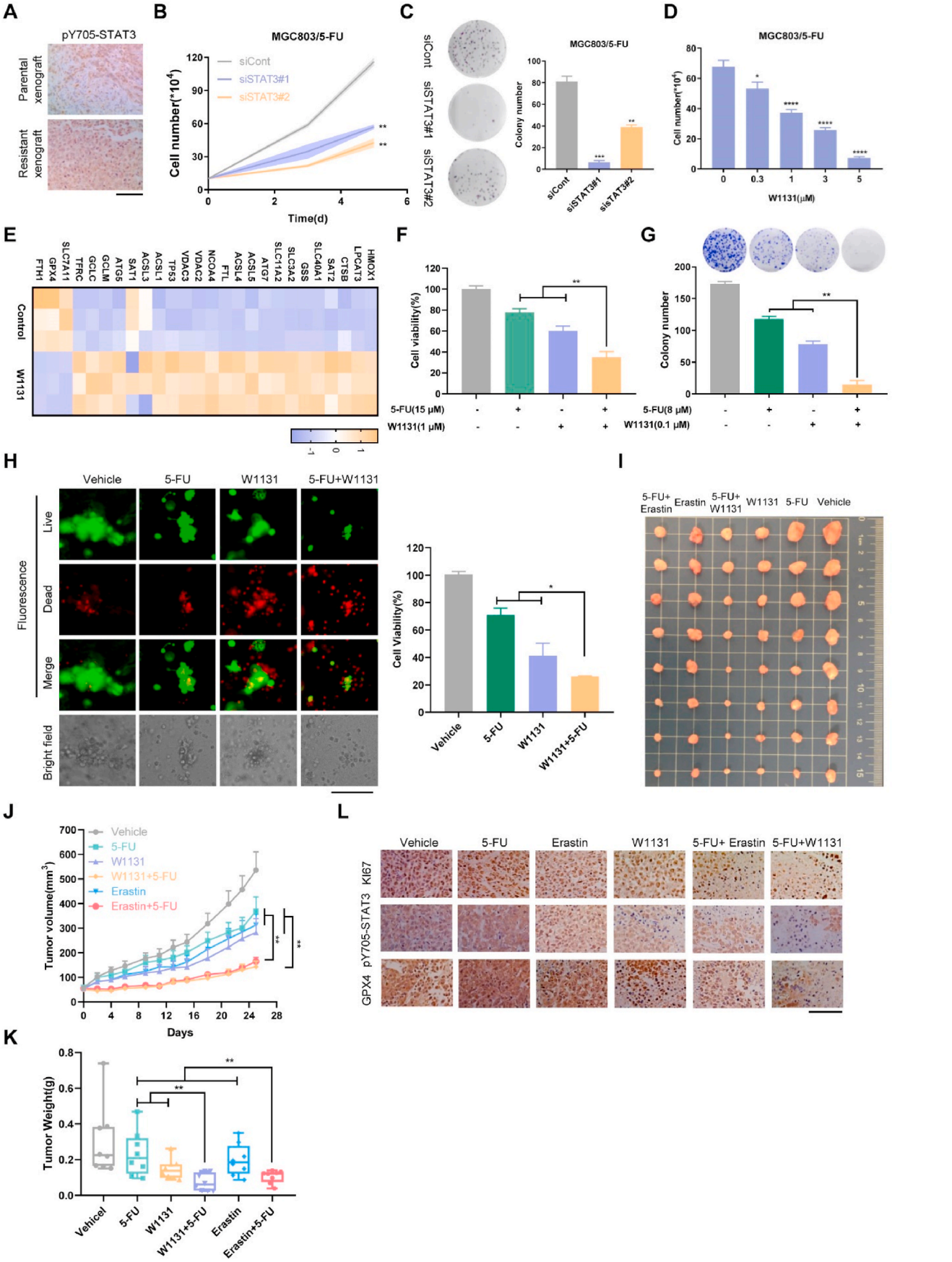

(caption on next page)

Fig. 8. W1131 alleviates chemotherapy resistance in multiple models of gastric cancer A: IHC analysis of pY705-STAT3 expression in MC803 and MGC803/5-FU xenografts. Scale bars = 100 μm. **B**: MGC803/5-FU were transfected with siRNAs against STAT3 (siSTAT3#1 and siSTAT3#2) or control siRNA (second). Viable cells were counted at indicated time points. **C**: MGC803/5-FU cells were infected as in (B).14 days later, colonies were counted. **D**: MGC803/5-FU cells were treated with vehicle (DMSO) or the indicated concentrations of W1131 for 72 h. Cells were harvested for determining cell growth by counting viable cells. **E**: RT-PCR analysis of ferroptosis-related genes with cDNA microarrays in MGC803/5-FU cells treated with vehicle (DMSO) or W1131(3 μM) for 48 h. Heatmap indicated the mRNA expression level of ferroptosis-related genes(Z-score). **F**: MGC803/5-FU cells were treated with 5-FU (15 μM) and/or W1131(1 μM) as indicated. After 72 h, total viable cells were counted with a Coulter cell counter. **G**: MGC803/5-FU cells were treated with 5-FU (8 μM) and/or W1131 (0.1 μM) as indicated. 14 days later, colonies were counted. **H**: PDX-derived organoids were treated with DMSO, 5-FU, W1131, erastin, and their combination, as indicated. Four days later, representative images were taken under a fluorescence microscope (top three rows) or standard light microscope (bottom row). Scale bars = 100 μm. Four days later, cell viability in organoids was measured with CellTiter-Glo. **I–K**: BALB/c-nu/nu mice bearing the MGC803/5-FU xenografts (n = 6 mice per group) received the vehicle, 5-FU (i.p., 20 mg/kg, once every other day), W1131 (i.p., 3 mg/kg, once daily), erastin (i.p., 20 mg/kg, once every other day) and their combination, as indicated. Mean tumor volume ± standard error of the mean (SEM) (J), representative tumor images (I), and mean tumor weight ± SEM (K) are shown. **L**: H&E and IHC images of the indicated proteins in the randomly selected PDX tumor section. Scale bars = 100 μm. *$P < 0.05$, **$P \leq 0.01$, ***$P < 0.001$, ****$P \leq 0.0001$. n = 3. Student's t-test.

Acknowledgments

We thank professor Ruibo Wu for his valuable suggestions for molecular docking studies and professor Jinping Lei for bioinformatic analysis. This work was supported by the National Natural Science Foundation of China (81973359, 21977128, U21A20419), Guangdong Basic and Applied Basic Research Foundation (2022A1515012204), Guangzhou Basic, and Applied Basic Research Foundation (202002030408, 202103000097). Jilin Province Science and Technology Development Project (20210204055YY), National Engineering and Technology Research Center for New drug Druggability Evaluation (Seed Program of Guangdong Province, 2017B090903004), National Major Special Projects for the Creation and Manufacture of New Drugs (2019ZX09301104), Local Innovative and Research Teams Project of Guangdong Pearl River Talents Program (2017BT01Y093), The Fundamental Research Funds for the Central Universities, Sun Yat-sen University (2021qntd44), Key-Area Research and Development Program of Guangdong Province (2020B1111110003), Guangdong Provincial Key Laboratory of Construction Foundation (2019B030301005) are also appreciated.

Appendix A. Supplementary data

Supplementary data to this article can be found online at https://doi.org/10.1016/j.redox.2022.102317.

References

[1] E.C. Smyth, et al., Gastric cancer, Lancet 396 (2020) 635–648.
[2] L. Shen, et al., Management of gastric cancer in Asia: resource-stratified guidelines, Lancet Oncol. 14 (2013) e535–e547.
[3] T. Wang, et al., JAK/STAT3-Regulated fatty acid beta-oxidation is critical for breast cancer stem cell self-renewal and chemoresistance, Cell Metabol. 27 (2018) 136–150, e5.
[4] S.T. Kim, et al., Comprehensive molecular characterization of clinical responses to PD-1 inhibition in metastatic gastric cancer, Nat. Med. 24 (2018) 1449–1458.
[5] S.J. Dixon, et al., Ferroptosis: an iron-dependent form of nonapoptotic cell death, Cell 149 (2012) 1060–1072.
[6] B.R. Stockwell, et al., Ferroptosis: a regulated cell death nexus linking metabolism, redox biology, and disease,, Cell 171 (2017) 273–285.
[7] X. Chen, et al., Iron metabolism in ferroptosis, Front. Cell Dev. Biol. 8 (2020) 590226.
[8] X. Chen, et al., Broadening horizons: the role of ferroptosis in cancer, Nat. Rev. Clin. Oncol. 18 (2021) 280–296.
[9] J. Tsoi, et al., Multi-stage differentiation defines melanoma subtypes with differential vulnerability to drug-induced iron-dependent oxidative stress, Cancer Cell 33 (2018) 890–904, e5.
[10] V.S. Viswanathan, et al., Dependency of a therapy-resistant state of cancer cells on a lipid peroxidase pathway, Nature 547 (2017) 453–457.
[11] M.J. Hangauer, et al., Drug-tolerant persister cancer cells are vulnerable to GPX4 inhibition, Nature 551 (2017) 247–250.
[12] J.L. Roh, et al., Induction of ferroptotic cell death for overcoming cisplatin resistance of head and neck cancer, Cancer Lett. 381 (2016) 96–103.
[13] Y. Mou, et al., Ferroptosis, a new form of cell death: opportunities and challenges in cancer, J. Hematol. Oncol. 12 (2019) 34.
[14] C. Wang, et al., Stearoyl-CoA desaturase 1 (SCD1) facilitates the growth and anti-ferroptosis of gastric cancer cells and predicts poor prognosis of gastric cancer, Aging (Albany NY) 12 (2020) 15374–15391.
[15] H. Zhang, et al., CAF secreted miR-522 suppresses ferroptosis and promotes acquired chemo-resistance in gastric cancer, Mol. Cancer 19 (2020) 43.
[16] J.F. Bromberg, et al., Stat3 as an oncogene, Cell 98 (1999) 295–303.
[17] L.B. Mora, et al., Constitutive activation of Stat3 in human prostate tumors and cell lines: direct inhibition of Stat3 signaling induces apoptosis of prostate cancer cells, Cancer Res. 62 (2002) 6659–6666.
[18] J.I. Song, J.R. Grandis, STAT signaling in head and neck cancer, Oncogene 19 (2000) 2489–2495.
[19] W.M. Burke, et al., Inhibition of constitutively active Stat3 suppresses growth of human ovarian and breast cancer cells, Oncogene 20 (2001) 7925–7934.
[20] L.M. Judd, et al., STAT3 activation regulates growth, inflammation, and vascularization in a mouse model of gastric tumorigenesis, Gastroenterology 131 (2006) 1073–1085.
[21] C.Y. Sun, et al., Targeting STAT3 inhibition to reverse cisplatin resistance, Biomed. Pharmacother. 117 (2019) 109135.
[22] L.V. Sequist, et al., Genotypic and histological evolution of lung cancers acquiring resistance to EGFR inhibitors, Sci. Transl. Med. 3 (2011), 75ra26.
[23] Q. Zheng, et al., A novel STAT3 inhibitor W2014-S regresses human non-small cell lung cancer xenografts and sensitizes EGFR-TKI acquired resistance,, Theranostics 11 (2021) 824–840.
[24] K.S. Chun, et al., Perspectives regarding the intersections between STAT3 and oxidative metabolism in cancer, Cells (2020) 9.
[25] H. Gao, et al., Ferroptosis is a lysosomal cell death process, Biochem. Biophys. Res. Commun. 503 (2018) 1550–1556.
[26] Q. Liu, K. Wang, The induction of ferroptosis by impairing STAT3/Nrf2/GPx4 signaling enhances the sensitivity of osteosarcoma cells to cisplatin,, Cell Biol. Int. 43 (2019) 1245–1256.
[27] S. Doll, et al., ACSL4 dictates ferroptosis sensitivity by shaping cellular lipid composition, Nat. Chem. Biol. 13 (2017) 91–98.
[28] C.W. Brown, et al., The alpha6beta4 integrin promotes resistance to ferroptosis,, J. Cell Biol. 216 (2017) 4287–4297.
[29] W.S. Yang, et al., Regulation of ferroptotic cancer cell death by GPX4, Cell 156 (2014) 317–331.
[30] J.P. Friedmann Angeli, et al., Inactivation of the ferroptosis regulator Gpx4 triggers acute renal failure in mice, Nat. Cell Biol. 16 (2014) 1180–1191.
[31] Y. Xie, et al., Ferroptosis: process and function, Cell Death Differ. 23 (2016) 369–379.
[32] X. Chen, et al., Ferroptosis: machinery and regulation, Autophagy (2020) 1–28.
[33] M. Conrad, H. Sato, The oxidative stress-inducible cystine/glutamate antiporter, system x (c) (-) : cystine supplier and beyond,, Amino Acids 42 (2012) 231–246.
[34] P. Koppula, et al., Amino acid transporter SLC7A11/xCT at the crossroads of regulating redox homeostasis and nutrient dependency of cancer, Cancer Commun. (2018) 38.
[35] M. Conrad, D.A. Pratt, The chemical basis of ferroptosis,, Nat. Chem. Biol. 15 (2019) 1137–1147.
[36] H. Sato, et al., Redox imbalance in cystine/glutamate transporter-deficient mice, J. Biol. Chem. 280 (2005) 37423–37429.
[37] M. Menotti, et al., Wiskott-Aldrich syndrome protein (WASP) is a tumor suppressor in T cell lymphoma, Nat. Med. 25 (2019), 130-+.
[38] Z. Qiang, et al., Nrf2 and STAT3 alleviates ferroptosis-mediated IIR-ALI by regulating SLC7A11, Oxid. Med. Cell. Longev. 2020 (2020) 5146982.
[39] H.B. Zhou, et al., Structure-based Discovery of SD-36 as a potent, selective, and efficacious PROTAC degrader of STAT3 protein, J. Med. Chem. 62 (2019) 11280–11300.
[40] P. Cimmperman, et al., A quantitative model of thermal stabilization and destabilization of proteins by ligands,, Biophys. J. 95 (2008) 3222–3231.
[41] D.M. Molina, et al., Monitoring drug target engagement in cells and tissues using the cellular thermal shift assay, Science 341 (2013) 84–87.
[42] P. Yue, et al., Hydroxamic acid and benzoic acid-based STAT3 inhibitors suppress human glioma and breast cancer phenotypes in vitro and in vivo, Cancer Res. 76 (2016) 652–663.
[43] H. Zhong, H. Yin, Role of lipid peroxidation derived 4-hydroxynonenal (4-HNE) in cancer: focusing on mitochondria, Redox Biol. 4 (2015) 193–199.
[44] C.S. Fuchs, et al., Adjuvant chemoradiotherapy with epirubicin, cisplatin, and fluorouracil compared with adjuvant chemoradiotherapy with fluorouracil and leucovorin after curative resection of gastric cancer: results from CALGB 80101 (alliance), J. Clin. Oncol. 35 (2017) 3671–3677.

[45] Z. Song, et al., Progress in the treatment of advanced gastric cancer, Tumour Biol. 39 (2017), 1010428317714626.
[46] S. Azwar, et al., Recent Updates on Mechanisms of Resistance to 5-Fluorouracil and Reversal Strategies in Colon Cancer Treatment, 2021, p. 10. Biology (Basel).
[47] N.N. Danial, S.J. Korsmeyer, Cell death: critical control points, Cell 116 (2004) 205–219.
[48] M. Manoochehri, et al., Down-regulation of BAX gene during carcinogenesis and acquisition of resistance to 5-FU in colorectal cancer, Pathol. Oncol. Res. 20 (2014) 301–307.
[49] W. Wang, et al., Andrographolide reversed 5-FU resistance in human colorectal cancer by elevating BAX expression, Biochem. Pharmacol. 121 (2016) 8–17.
[50] C. Yang, et al., Apigenin enhances apoptosis induction by 5-fluorouracil through regulation of thymidylate synthase in colorectal cancer cells, Redox Biol. (2021) 47.
[51] W.T. He, et al., Curcumin reverses 5-fluorouracil resistance by promoting human colon cancer HCT-8/5-FU cell apoptosis and down-regulating Heat shock protein 27 and P-glycoprotein, Chin. J. Integr. Med. 25 (2019) 416–424.
[52] C. Mao, et al., DHODH-mediated ferroptosis defence is a targetable vulnerability in cancer, Nature 593 (2021), 586-+.
[53] K. Linher-Melville, G. Singh, The complex roles of STAT3 and STAT5 in maintaining redox balance: lessons from STAT-mediated xCT expression in cancer cells,, Mol. Cell. Endocrinol. 451 (2017) 40–52.
[54] L. Jiang, et al., Ferroptosis as a p53-mediated activity during tumour suppression, Nature 520 (2015), 57-+.
[55] X. Zhang, et al., Orally bioavailable small-molecule inhibitor of transcription factor Stat3 regresses human breast and lung cancer xenografts, Proc. Natl. Acad. Sci. U. S. A. 109 (2012) 9623–9628.
[56] J. Schust, et al., Stattic: a small-molecule inhibitor of STAT3 activation and dimerization, Chem. Biol. 13 (2006) 1235–1242.
[57] K. Siddiquee, et al., Selective chemical probe inhibitor of Stat3, identified through structure-based virtual screening, induces antitumor activity, Proc. Natl. Acad. Sci. USA 104 (2007) 7391–7396.
[58] S.F. Hussain, et al., A novel small molecule inhibitor of signal transducers and activators of transcription 3 reverses immune tolerance in malignant glioma patients,, Cancer Res. 67 (2007) 9630–9636.
[59] X. Zhang, et al., A novel inhibitor of STAT3 homodimerization selectively suppresses STAT3 activity and malignant transformation,, Cancer Res. 73 (2013) 1922–1933.
[60] X. Zhang, et al., A novel small-molecule disrupts Stat3 SH2 domain-phosphotyrosine interactions and Stat3-dependent tumor processes,, Biochem. Pharmacol. 79 (2010) 1398–1409.
[61] K. Matsuno, et al., Identification of a new series of STAT3 inhibitors by virtual screening, ACS Med. Chem. Lett. 1 (2010) 371–375.
[62] D.Y. Oh, et al., Phase I study of OPB-31121, an oral STAT3 inhibitor, in patients with advanced solid tumors, Cancer Res. Treat. 47 (2015) 607–615.
[63] J.C. Bendell, et al., Phase 1, open-label, dose-escalation, and pharmacokinetic study of STAT3 inhibitor OPB-31121 in subjects with advanced solid tumors, Cancer Chemother. Pharmacol. 74 (2014) 125–130.
[64] M. Ogura, et al., Phase I study of OPB-51602, an oral inhibitor of signal transducer and activator of transcription 3, in patients with relapsed/refractory hematological malignancies, Cancer Sci. 106 (2015) 896–901.
[65] D. Tang, et al., Ferroptosis: molecular mechanisms and health implications, Cell Res. 31 (2021) 107–125.